UCLouvain

École polytechnique de Louvain

Computed tomographic analysis of a new eco-circular composite material for construction application

A material science project

Author: **Alexandre DE BRIEY**
Supervisor: **Thomas PARDOEN**
Readers: **Thomas PARDOEN, Joao ALMEIDA, Sophie TRACHTE**
Academic year 2021–2022
Master [120] in Chemical and Materials Engineering

Acknowledgements

First of all, I would like to thank my framer, PHD Mélanie Horvath for guiding me throughout the realization of this thesis. Her availability and advice were crucial for the achievement of this work. I am very grateful to her for giving me the opportunity to spend last year in her research group at EPL and for giving me my first insights to this field of research. I have learned a lot from her ability to challenge new and existing ideas and focus on the impact of different concepts.
I would also like to thank my supervisor, prof. Thomas Pardoen for the opportunity to write this thesis and for his help throughout the process of this thesis.
I would like to express my sincere gratitude to Dr. Grzegroz Pika and Dr. Florent Hannard for the time they dedicated to the many meetings we have had. Their professionalism and knowledge made these meetings very constructive and always helped me to move forward with my work.
Eloïse and Alexis, two other master's thesis students with some knowledge of civil engineering, greatly contributed to my experience with the research team. I found it very motivating and rewarding to be part of a group of like minded individuals passionate about ecological threats linked to construction developments.
Many thanks also go to Prof. Joao Almeida, who along with Prof. Sophie Trachte, agreed to be part of the jury of this thesis.
Last but not least, I would like to warmly thank my friends for their unconditional support. I am grateful for the remarkable value they place on education, which surely accounts a great deal to where I am today.

Abstract

The construction industry is not only considered the largest contributor to waste, but also the leader in environmental pollution. Instead of recycling, landfill is currently the primary method of dealing with waste generated by the construction sector in the majority of the world. Reducing the construction and demolition is not a solution, as the economic development of each country depends largely on construction projects. The best way to minimize waste generated by the construction industry is to employ eco-friendly materials and construction techniques to build sustainable buildings.

This thesis aims to design a healthy and sustainable material for construction with a low energy production process, composed of paper from the recycling industry to which two additives are joined: hydraulic lime and recycled crushing sand. The experimental part of this thesis aims to test and compare various compositions with a specific characteristic in order to find the optimal composition for a material to serve in the construction industry. Microstructure is the prime factor controlling the mechanical property of materials. Therefore, knowing the microstructure of the material helps to understand its macroscopic response and to adapt the materials accordingly. Microstructural images of each composition are computed using X-ray micro-tomography and a visual representation of the individual material components, as well as analytic data on the microstructure, is provided. Additional information is then given on the possible impact of the porosity on the properties and on the role and correlation of the different phases between them. Finally, an in-situ compression tomography analysis is provided. The impact of the microstructure on the properties obtained in laboratory tests is then discussed, followed by a summary of the impact of each feature on the material.

Contents

1 Introduction **6**
- 1.1 Context . . . 6
- 1.2 Where it all began . . . 7
- 1.3 Objectives . . . 8

2 State of the art **10**
- 2.1 Recycled materials for construction applications . . . 10
  - 2.1.1 Plastic composites . . . 10
  - 2.1.2 Crushed sand recycled in bedding mortars . . . 12
- 2.2 Paper-based materials in construction applications . . . 13
  - 2.2.1 Papercrete . . . 13
  - 2.2.2 Honext . . . 14
- 2.3 Use of tomography in construction materials . . . 16
  - 2.3.1 Introduction to tomography . . . 16
  - 2.3.2 Use of CT scan technology in concrete . . . 17
- 2.4 State of knowledge . . . 19

3 Methodology **21**
- 3.1 Sample preparation . . . 21
  - 3.1.1 Materials . . . 21
  - 3.1.2 Initial process . . . 23
  - 3.1.3 Molding process . . . 25
- 3.2 Variable parameters . . . 27
- 3.3 First campaign . . . 29
  - 3.3.1 Samples, parameters and processes . . . 29
  - 3.3.2 Mechanical tests . . . 32
  - 3.3.3 Results . . . 33
- 3.4 Second campaign . . . 36
  - 3.4.1 Nomenclature . . . 36
  - 3.4.2 Variable parameters . . . 36
  - 3.4.3 Choice of samples to analyse . . . 39

4 Computed tomography analysis **41**
4.1 Image processing and segmentation 41
4.2 Volume fraction 44
4.3 Porosity analysis 46
4.3.1 Percolation 46
4.3.2 Void orientation 47
4.3.3 Size of voids 50
4.4 In-situ compression 52
4.4.1 Graphical analysis 52
4.4.2 Image segmentation analysis 52
4.4.3 DVC analysis 53

5 Results **55**
5.1 Segmentation 55
5.2 Volume fraction 61
5.3 Porosity analysis 64
5.3.1 Percolation 64
5.3.2 Void orientation 65
5.3.3 Size of voids 68
5.4 In-situ compression 70
5.4.1 Graphical analysis 70
5.4.2 Image segmentation analysis 71
5.5 DVC analysis 74

6 Discussion **76**
6.1 Link microstructural analysis with laboratory tests 76
6.1.1 Segmentation 76
6.1.2 Volume fraction 80
6.1.3 Porosity analysis 81
6.1.4 Compressibility of the material 83
6.2 Summary properties 85
6.3 Possible improvements 87

7 Conclusion **88**

A Segmentation **89**
A.1 Median filter 89

B Results **90**

C Volume fraction **94**
C.1 Image analysis 94
C.2 Experimental analysis 95

D Porosity analysis **96**
D.1 Void orientation 96
D.2 Pores size distribution 97

E Phase correlation **98**
E.1 Methodology 98
E.1.1 Method 1: Neighbour count 98
E.1.2 Method 2: Modified PCF (bimodal with centroids) and method of quadrats 99
E.2 Results 102
E.2.1 Method 1: Neighbour count 102
E.2.2 Method 2: Modified PCF (bimodal with cen- troids) and method of quadrats 102

F Compressibility **103**
F.1 Poisson's ratio 103

Chapter 1

Introduction

1.1 Context

Construction and demolition waste accounts for more than a third of all waste generated in the European Union [27]. Indeed, important construction and demolition waste are generated every year during the construction, renovation and demolition of buildings and infrastructures. The construction industry is not only considered to be the most important contributor to waste, but also the primary cause of environmental pollution [18]. It is reported that the total amount of waste generated by the construction sector worldwide exceeds 10 billion tons each year, of which the United States produces about 700 million tons and the European Union more than 800 million tons [5].

Compared to recycling, landfilling is currently the main treatment method for construction and demolition waste in many parts of the world. It is estimated that about 35% of this waste is landfilled worldwide [8]. However, the economic development of each country is largely dependent on construction projects and the construction industry provides numerous job opportunities, economic contributions, and serves as the foundation for other businesses [27].

Therefore, there is an urgent need to minimize the environmental impacts of waste generated by the construction sector without losing all the benefits provided. In response to this problem, the "2030 Agenda for Sustainable Development of the United Nations General Assembly", approved in 2015 by the UN member countries, established the "Sustainable Cities" model. This model plan to reduce the negative environmental impact of cities by 2030, paying special attention to the management and recycling of generated waste. Besides, eco-friendly materials are most adapted to the construction of green buildings. This is why PhD student Mélanie Horvath

imagined (during a group work within the framework of one of her architectural courses) the "paper brick", a composite material resulting mostly from recycling [11]. The paper brick is a new building material that takes into account the various environmental, economic and social issues involved. The first objective of this TFE is to study the development of this "paper brick" and to deepen the research on this material through applications in materials science using computed tomography analysis.

1.2 Where it all began

In the 2017/2018 academic year, a simple lesson on "Materiality and eco-design" was taught in the faculty of architecture, architectural engineering and urban planning of the Université Catholique de Louvain. During the lesson, Mélanie and one of her colleagues, Fanny Dufour, were asked to implement an eco-circular material for the cladding of a front module. After some thorough thinking, they found an ideal solution: A brick with paper as its main component. The objective was to conceive a healthy and sustainable material, so it is essentially composed of paper fibres resulting from recycling, to which two additives are added: lime and sand. The paper would offer lightness and an insulating power to the material, the lime as the binder would offer greater resistance to water and the sand would offer mechanical strength. Following the interest of several teachers in this material, they were encouraged to further pursue research and made this subject their master's thesis.

During their master thesis, numerous experimental tests have been carried out, including water absorption tests, fire resistance tests, 3-point bending test, compression tests, creep tests and thermal conductivity tests. The conclusions of their master thesis are that the results were surprising and exceeded the expectations they had when they started their final study. Due to the successful results of her work, Mélanie is given the opportunity to further develop her work by doing a 4-year doctorate, with the help of PhD Thomas Pardoen. She seized this opportunity and started her PhD at the Université Catholique de Louvain, where I first met her. Together, and with the help of Alexis Masarweh and Eloïse Denis, we started to study this paper-brick more in depth during the 2021/2022 academic year.

1.3 Objectives

The main objective of this project is to create a sustainable composite to limit the environmental impact in the construction sector. To be effective, the composite must meet major characteristics:

- Low environmental footprint.
- Sufficient mechanical characteristics (strength, modulus, fracture resistance, creep resistance, ...).
- Sufficient thermal characteristics.
- Available and profitable.
- Fire & water resistance.

The work is clear: to help Mélanie optimize her composite as much as possible by testing and analyzing samples with different characteristics. Indeed, there are different ways to treat the composite (see section 3.2). For example, we can adjust the proportions of different materials constituting the compound, choose a different type of paper fibre, lime or sand, etc. Sometimes a method will be used to create defects (such as adding too much water) and analyse the results.

The experimental part of this thesis aims to test and compare the various compositions created to have a better idea of the influence of all parameters on the composite, and finally find the composition that best optimises the material. This thesis is realised in parallel with the master thesis of Alexis Mazarweh and Eloïse Denis, two master students in civil engineering. Indeed, Alexis and Eloise focus on processing and analysing laboratory tests to quantify mechanical, acoustic and thermal performances of the material, while this thesis tries to explain the results of the different mechanical tests by microstructural analysis. The microstructural analysis is done with the help of x-ray computed tomography with the Thermofisher's Avizo software. In many cases, the combined use of computed tomography scans (CT-scans) and mechanical or thermal characterisation tests of the composite material allows relationships to be established between the microstructure and its macroscopic response.

The organisation of this work is as follows: Images received by tomography are in shades of grey. These images are then first processed and segmented in order to have a clear distinction between compounds in the material. A first visual inspection and analysis is then performed, and the role and correlation of the different phases are discussed. The volume fraction of each compound in more

than 19 samples is then computed. Subsequently, more information will be given on the porosity of the samples and emphasis is given to the relationship between mechanical properties and volume porosity. Moreover, an in-situ compression analysis is provided, supported by image segmentation. Finally, links are discussed between the results of the laboratory tests performed by Alexis and Eloise and the results of the microstructural analysis performed during this thesis.

Chapter 2

State of the art

2.1 Recycled materials for construction applications

Concrete blocks play an important role in the construction industry. Concrete blocks have been used in the making of various buildings, retaining walls and more. Unfortunately, some of these technologies have detrimental consequences on the environment. For instance, the production of cement will contribute to high emissions of harmful gases such as carbon dioxide that can be hazardous to human's health. Therefore, many engineers are trying to find a new alternative to deal with this environmental problem [20]. One of the main ideas is to minimize concrete production by mixing concrete with recycled materials to create new components for the construction industry. Through technological innovation, waste is incorporated (again and again) into the production processes of new products and/or materials (towards the "zero-waste" objective). Two of the most widespread waste products found on earth are plastic and construction and demolition wastes. Some engineers have already reflected upon the issue and invented their own concrete blocks made from recycled material. These concrete blocks may be used as alternatives to bricks and traditional stones in construction and buildings.

2.1.1 Plastic composites

The use of recycled plastic aggregates in concrete is an option for plastic disposal and ultimately reduces plastic pollution in the environment. Some research intends to study the possibility of using recycled plastic water bottles within the local concrete blocks for building construction. Using recycled plastic in concrete reduces the weight of a cube up to 15%. Therefore, this type of stone is sometimes preferred due to its smaller weight and ease of transfer compared to bricks. They can be

used in different places such as interior walls, exterior walls bearing and columns, compound walls, retaining walls, etc. Moreover, they provide an advantage of uniform quality as well as speeding in construction. As they consume less cement and involve fewer laborers, they are less expensive. For all these reasons, plastic-concrete blocks are vastly used in building construction and thermal insulation of walls [24]. However, the plastic composites can contain maximum 20% recycled plastic aggregates in the mix in order to still sustain the properties of concrete needed in construction applications [28]. This leaves another 80 % of polluting agents for each brick manufactured.

Figure 2.1: Concrete block containing recycled plastic bottles [24].

2.1.2 Crushed sand recycled in bedding mortars

Construction and demolition waste can be classified into two categories: usable and non-usable waste. Non-usable wastes are those that are contaminated with hazardous substances, so their use is restricted by environmental regulations. In the usable waste group, concrete, ceramic, masonry, and mortar waste is mainly found. In general, these wastes have been treated to produce fine and coarse aggregates. These can be incorporated into mortars and concrete mixtures as a replacement (partial or total) for natural aggregates, as shown in figure 2.2 [23]. Recycling waste generated on construction sites reduces the risk of its contamination, and this is a more sustainable and economical alternative for the builder. In this manner, it reduces costs and carbon emissions attributable to transportation. The use of recycled sand for example in bedding masonry mortar is an interesting alternative. These mortars have no structural function, consume large amounts of fine aggregate, are not subject to the presence of moisture and can be produced with recycled aggregate from ceramic wastes [19]. However, the production of recycled aggregates does not represent a solution for the exploitation of construction wastes worldwide, mainly due to the low commercial competitiveness they possess when compared to the economic (non-environmental) cost with that of natural aggregates in many cities and countries.

Figure 2.2: Recycling process of crushed sand into concrete blocks [23].

2.2 Paper-based materials in construction applications

Forests are burning all over the world and 15,3 billion trees are still cut down each year [14]. In addition, paper is one of the most frequent types of waste found in almost all areas of activity and is a major source of cellulose fibres. In various forms (quality paper, mixed paper, newspaper and journals, undulated cardboard), paper represents about 41% of all household waste generated today. This is why paper recycling should be an opportunity to reduce the impact on forest and on the environment [1]. Bricks made of paper fibres agglomerated with cement are an inexpensive material, with good thermal insulation, resistance, produced through the recovery of paper waste. This makes recycling paper in building materials both beneficial for the construction industry and for the environment.

2.2.1 Papercrete

Papercrete (paper + (con)-crete) is a building material that consists of re-pulped paper fibres. First patented in 1928, it was revived during the 1980s. The design of the mixing ratio of papercrete has been studied by several authors [22] but waste paper is the main ingredient of papercrete and the additional materials are ordinary Portland cement, fine sand, fly ash, and some additives depending on different studies (for example Cem-FILL Anti-Crack HD Glass Fibres [25] or Ground Granulated Blast Furnace Slag (Ggbs) [2]).

Figure 2.3: Papercrete blocks for commercialisation [25].

The material has different qualities depending on the dosage of paper, cement and

any other materials and on the type of paper, the preparation used, the use of a press or not, etc.

These bricks have a significant advantage: as the waste is recycled, it reduces the landfill and pollution. Consequently, they are considered sustainable and low-polluting. They are lightweight, and the total cost will be reduced by 20% to 50%. The papercrete bricks have elastic behaviors, and they are less brittle than concrete bricks. They are exceptional thermal insulators and have very good acoustic properties. However, they have also some drawbacks: papercrete bricks are suitable for non-load bearing walls only. Papercrete should not be used for external walls and near-ground walls due to its high water absorption capacity [34]. Although perceived as an environmentally friendly material due to the significant recycled content, this is offset by the presence of cement.

2.2.2 Honext

Barcelona-based company Honext has developed a waste-reclaiming process that turns cellulose leftovers of unusable paper sludge and cardboard waste residues into a ready-to-use, fully recyclable material. Their raw materials come from paper mills and waste disposal facilities. They use this unusable paper sludge and cardboard waste to make board material, using a mix of enzymes, non-toxic additives, heat and pressure. The material does not contain non-recyclable binding resins and does not emit harmful particles. A mixture of 50 to 75 % paper sludge and 25 to 50 % cardboard waste is used. By adding certain enzymes during the production process, Honext creates stronger bindings between the short cellulose fibres without having to use non-recyclable resins.

Figure 2.4: Honext panels for construction application [21].

The board material can be used for interior partitioning or cladding. It has similar properties to traditional materials used for such applications, with the particularity of being lighter, more flexible and with better sound absorption than materials like drywall [21]. However, this material is reserved exclusively for board-materials and cannot be used to replace cement in all circumstances.

A table showing the principal properties of the materials analyzed is provided (table 2.1). All these promising breakthroughs justify our research intended as a great contribution to the development of innovative building materials with limited environmental and health impact.

	Compressive strength [N/mm^2]	Density [kg/m^3]	Modulus [GPa]	Thermal conductivity [W/mK]
Polymer concrete	13	2254	11	2
Bedding mortars	11.83	1980	1.68	[-]
Papercrete	1.12	382	8	0.08
Honext	14	540	3.2	0.096

Table 2.1: Comparative table of main properties of different recycled composites for construction application.

2.3 Use of tomography in construction materials

2.3.1 Introduction to tomography

It is well-known that the microstructure of materials largely determines their mechanical and physical attributes and behavior. Therefore, imaging the inner structure and morphological characteristics of materials is of paramount importance in material design and engineering. For this reason, engineers created radiographs working with electromagnetic waves, where the wavelength of the applied radiation determines the scale of the features investigated. Scanning electron microscopy (SEM) for example, provides a good resolution (nanometer scale) but only in 2D. 2D radiographs can confirm the existence of cracks, discontinuities, pores, or structural errors, but 3D images can also help us localise them and identify their origin. Furthermore, three-dimensional (3D) imaging can reveal the volume, shape, spatial and size distribution, and connectivity of inhomogeneities (e.g. pores, different phases, cracks). To investigate 3D structure with SEM, the sample has to be sectioned. This destructive technique takes a lot of time and is limited to imaging a very small volume [32].

During this thesis, 3D imaging in a transmission electron microscope is performed, and it is called electron tomography. (Computed) Tomography (CT) is a nondestructive technique, based on the absorbing X-ray attenuation of materials, which allows the visualization of the internal microstructure of materials. Transmission images of the sample acquired from at least a hundred different angles can be reconstructed into a 3D model of the sample [31].

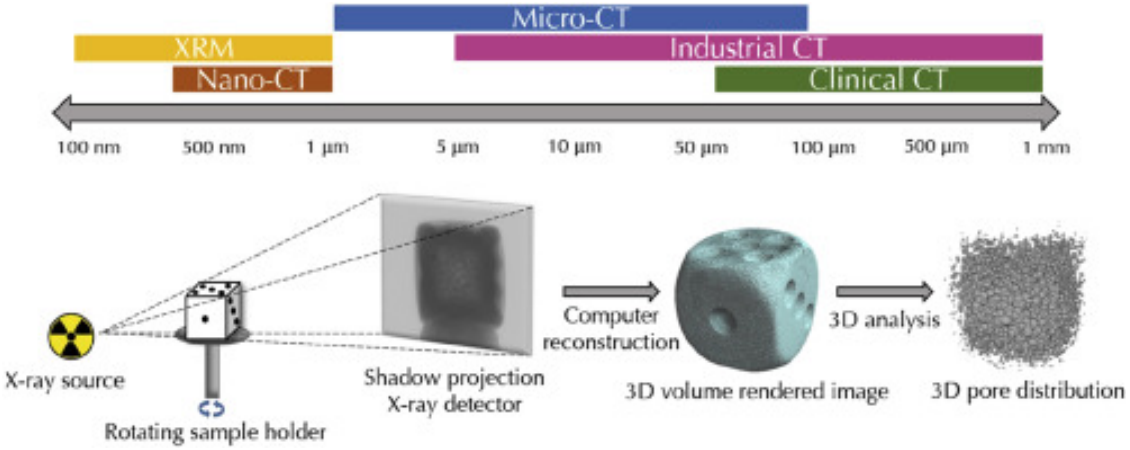

Figure 2.5: Classical working procedure of a tomograph [31].

X-ray tomography uses the ability of X-ray radiation to penetrate objects as shown in figure 2.5. As an object is penetrated, some of the incident radiation is absorbed. The longer the radiographic length of the object, the less radiation escapes from the opposite side. An X-ray detector (sensor) captures the escaping X-ray radiation as a two-dimensional radiographic image. Consequently, the absorption depends on the material. Several hundred two-dimensional radiographic images are made in sequence, with the measured object in various rotated positions (see figure 2.5). The three-dimensional information about the measured object contained in this series of images is extracted using a suitable mathematical process and is made available as a "voxel image". A voxel (volume pixel) is a 3D pixel that takes a value between 0 and 255, where the minimum density assumes a value equal to zero (black color) and the maximum density corresponds to a value equal to 255 (white color). Each voxel embodies the X-ray absorption by the measured object for a defined location in the measured volume. All the scans can then be assembled on a software (e.g. Aviso by Thermofisher).

Moreover, X-ray tomography being a non-destructive technique, it offers the possibility to record several scans of a single sample whose experimental environment (state of stress, temperature, etc...) is changing over time. The change in environmental condition can be applied ex-situ (e.g. straining the sample in a classical laboratory tensile testing device) and the sample re-installed on the tomograph for inspection but, for obvious practical reasons, it is much preferable to work in-situ with the sample constantly installed on the tomograph. The number and the type of in-situ experiments involving tomography have also widened considerably and various experimental environments have been studied (temperature, stress, corrosive environment etc.). Such in-situ experiments usually provide unique data which is essential for testing existing models or developing new ones [4].

2.3.2 Use of CT scan technology in concrete

In many cases, the combined use of CT scan and mechanical or thermal characterisation tests of the composite material allows relationships to be established between the microstructure and its macroscopic response. In general, in the case of a composite material, three phases may be distinguished: matrix, reinforcement, and pores or cracks. The behavior of the composite materials strongly depends on the distribution and the orientation of the reinforcement (the latter solely in the case of fibres) as well as the location in the pores and cracks. The composition of concrete, for example, is highly heterogeneous as its matrix is composed of different materials: cement, sand, and rough aggregate. The dosages of those elements are modified to obtain optimum mechanical capacities. Additionally, other types of materials are used to improve the performance of the concrete such as fibres

and additives to modify the internal structure of the material. Internally, what is generated is a matrix composed of aggregate fines and hydrated cement that cover the coarse aggregate as shown in figure 2.6 made with computed tomography analysis with the software Aviso.

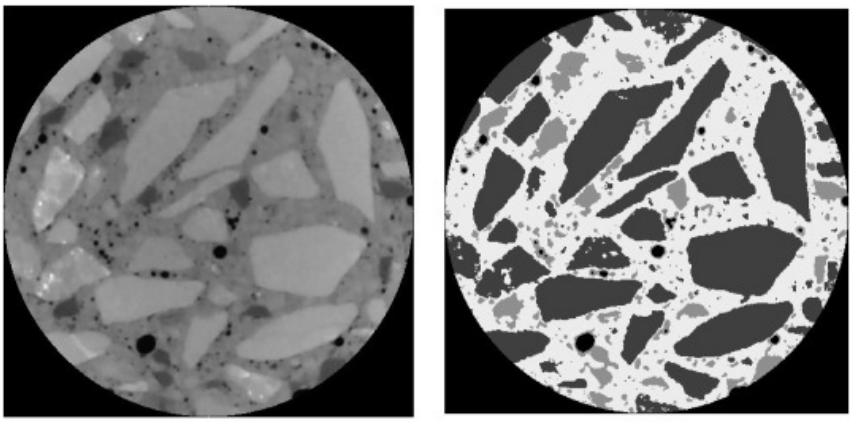

Figure 2.6: Concrete computed tomography analysis [16]. Figure b) is a reproduction of figure a) with a different tone of grayscale. The white parts are more dense compounds than the black parts.

Among the applications of the CT scan technology for the analysis of a concrete matrix, there are some experimental studies focused on recycled concretes [32] [15]. In these studies, concretes with equal percentages of 50% recycled aggregate (RCA) and 50% natural aggregates were analysed. The objective of the use of tomography is to evaluate the interfaces between both types of concretes. In addition, the porosity of each type of matrix is analysed. The identification of pores provides information on these internal gaps that the matrix presents. This information may relate to the size of the pores and their distribution within the specimen. Information may also be extracted on the sphericity of the pores as compared with a perfect sphere and finally, the spatial position of these pores within the matrix is computed. Images of the spatial distribution of the pores may be obtained using computerized topography image analysis and the use of post-processing tools including volumes, numbers of pores, positions within the specimen, and sphericity indexes. It is known that constituent type, constituent proportion, porosity content and void topology affect a porous medium's bulk strength and elasticity. These conclusions are also reflected in their works: a higher proportion of pores gives a lower elastic modulus (E) and a lower fracture toughness (R) [17].

2.4 State of knowledge

This entire section resumes the conclusions reached by Mélanie Horvath and Fanny Dufour during their thesis [11].

During their thesis, Mélanie and Fanny focused on six experimental tests to investigate the potential of their new finding. Mechanical tests (flexion, compression and creep tests), thermal tests (thermal conductivity), water absorption and fire resistance tests were performed, for different compositions. The proportion of paper and the type of lime and sand within are the main parameters to vary between different mixes. The main findings of these tests are summarised below.

- 3-point flexion test: Better properties appear with not-plasticised paper fibres and with hydraulic lime. Furthermore, blocks with high paper content have a suitable strength for this test.

- Compression test: It seems that the material is ductile and easily deformable. The results also show the importance of a complete drying in order to improve the compressive strength while keeping a maximum of paper and thus of recycled materials. In view of the results, it seems also interesting to favour bricks containing 50 to 60% paper, given that the 60% rate is a pivotal point and that rates higher than this seem to have lower compressive strength. **- Fire resistance test:** The conclusions of these tests are very positive, there is no need for the material to be covered with any fireproof coating.

- Thermal conductivity test: Paper bricks have a good thermal resistance. The use of these bricks in sufficient thickness would make it possible to reduce the quantity of insulation to be implemented in a construction.

- Adsorption of water test: As expected, the results are not conclusive. The resistances obtained are very low. However, these tests were carried out under extreme conditions, which do not represent the real climatic conditions in Belgium. The material will never be exposed to this amount of water.

To conclude, in most of the carried out tests, the brick containing **paper content between 40% and 60%** seems to be the best match. It seems that rates higher than this one have to be excluded if they were to be dedicated to an outside use. In particular, **hydraulic lime** plays an important role in the water absorption and fire reaction tests, as it forms a protective layer around the paper fragments. Thanks to its water and fire retardant properties, it prevents the paper from absorbing water or catching fire. Sand also helps lime in both properties. Later,

Mélanie discovered that river and **crushed sand** are more favorable than glass- and rock wool. The material works as an insulating mass and thus does not need to be accompanied by any insulation panel. This characteristic is a significant added value in addition to the fact that the product is made up mostly of part of recycled materials. The material could be used as facing bricks, interior walls or self-supporting blocks in a column-beam structure. Since these blocks are protected by an exterior coating, they will not come into contact with water and will not lose their resistance as in the absorption tests. It is also noticed that the material has great elasticity. It would be perfectly suitable for use in seismic zones (in the form of bricks and/or blocks).

Chapter 3

Methodology

3.1 Sample preparation

3.1.1 Materials

During the first weeks of the project, the objective was to collect the various material components required to make all samples needed during this thesis. In Melanie's previous work [12] [11], the idea of a composite material made of paper, lime and sand was developed. Paper offers lightness and insulating power to the material, the lime has a matrix role to bind the constituents together and to offer greater resistance to water and sand to boost mechanical strength. However, paper, lime and sand all exist in various forms. Indeed, paper can be found under different types of textures (cardboard, magazine, newspaper, quality paper etc.), sand can be found in different places with different granulate sizes (river sand, river sand, coarse sand, etc.), and there are different types of lime variations (Quick lime, Slaked lime, Fat lime, etc.). In order to perform a coherent and optimal research, only the most appropriate types of paper, sand and lime for our work are chosen. Thanks to Mélanie's previous experiences and analysis, the optimal type of material to reach our objectives is quickly deduced:

- **Paper:** Already used quality paper sheets.
- **Lime:** Hydraulic lime.
- **Sand:** Crushed sand recovered from construction and demolition waste.

After some experimentation, Mélanie realised that some sorts of paper such as magazine do not disintegrate in the mixture and due to some adhesives, they do not stick very well to the lime and sand. This type of paper is therefore excluded, as it is not useful for our work. After investigating all types of paper, the optimal

form of paper found is quality paper (e.g. sheets of paper books). To respect the environmental aspect of the project, only paper waste is used. Paper is collected in two different forms: on the one hand, as we do not have a fast enough confetti machine, confetti's are collected directly from the large-scale supermarket chain MAKRO. On the other hand, quality paper sheets found in our neighbourhood and in some libraries and universities, which are 100% recycled, are collected. They will then be transformed into medium and large fibres as shown in figure 3.8 thanks to shredding machines.

Crushed sand is obtained by crushing inert building waste, such as bricks, concrete, cement, ceramics or even porcelain, which are washed and screened to form sand with the same properties as river sand. The crushed sand used in this project is obtained from the Tradecowall-Recymex recycling and resource recovery center, located in St-Ghislain and is 100 % recycled. There is a real opportunity to use crushed sand instead of river sand (usually used in construction) because river sand is a resource under shortage. Furthermore, this reduces the waste from the construction sector, which is increasing every year and is still too little exploited as seen previously.

The third and final component is lime, which acts as a binder for the material. Lime is used instead of cement for its lower environmental impact. Indeed, it produces less grey energy during its manufacture and during its transport, since it is a local resource in Belgium [12]. Tradi'lime XHA is used from the company Cantillana. This type of lime belongs to the family of hydraulic limes. Hydraulic lime is chosen because it hardens partly by reaction with water (as shown in figure 3.1) and so differs from other types of lime that harden only by chemical reaction with carbon dioxide in the air.

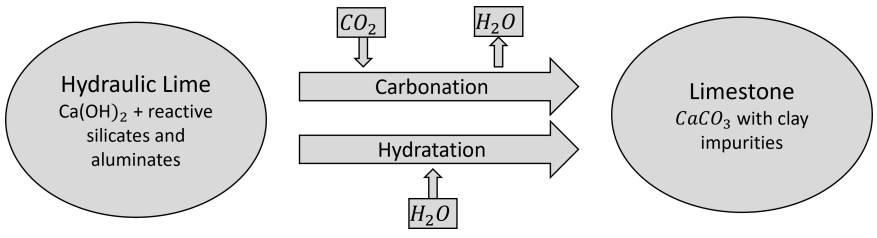

Figure 3.1: Reaction of hydraulic lime with water and carbon dioxide.

The quantities of materials shown in table 3.1 are collected:

Materials	Quantity [kg]	Source
Confettis	36	MAKRO
Medium fibers	84	Recycled paper shredded with shredding machine
Large fibers	60	Recycled paper shredded with shredding machine
River sand	32	Gedimat
Crushed sand	208	Tradecowall-Recymex
Lime	240	Gedimat-Tradi'chaux XHA

Table 3.1: Table of the different materials with the required quantities and source collected.

3.1.2 Initial process

Once the quantities needed for the process have been collected, sample preparation can start. It is done in six main steps, as shown in figure 3.2.

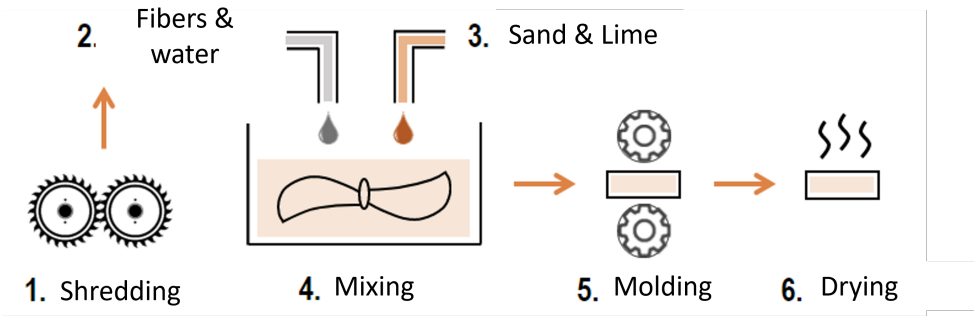

Figure 3.2: Producing process of the paper brick made by Mélanie (2020).

1. Shredding: paper sheets are shredded into medium and large bands (see figure 3.8 for more information about the size of the bands) using simple shredding machines.

2. Fibers & water: A required amount of dry fibers to create a composition is collected and soaked in water (see figure 3.3) in order to allow better decomposition. Paper soaking time is a variable parameter that will be part of our first campaign. The soaking of the paper is then initially set to 24 hours and takes place in a water basin at room temperature. After a full day of soaking, the paper bands are introduced into a mixer and are mixed and blended for two minutes in order to break up some pellets that were formed. The remaining pellets are broken up by hand. The objective is to have a good distribution of paper bands in the composite.

Figure 3.3: Soaking of paper in water basin (picture taken by Mélanie).

3. Sand and lime: Crushed sand followed by lime are added in required proportions into the mixture. The sand and lime are well distributed throughout the whole mixture in order to achieve an initial uniform distribution in the material (as shown in figure 3.4).

Figure 3.4: Distribution of sand on the mixed paper (picture taken by Mélanie).

4. Mixing: Mixing of the components can now start. The mixing duration is a variable parameter that is tested in our first campaign. Some water is added during the mix (which is also a variable parameter) to allow the reaction of lime and water to proceed. The resulting mixture is represented in figure 3.5 and looks like wet soil.

Figure 3.5: Mixing of the composite (picture taken by Mélanie).

5. Molding: Molding of the samples can now start. It is done manually in molds of appropriate shapes. See section 3.1.3 for more information about the process.

6. Drying: The molded samples are then dried at room temperature for about one month in order to get completely rid of all the water absorbed by the material during the process.

3.1.3 Molding process

The compound freshly released out of the mixer is manually put in molds with various shapes, as shown in figure 3.6.

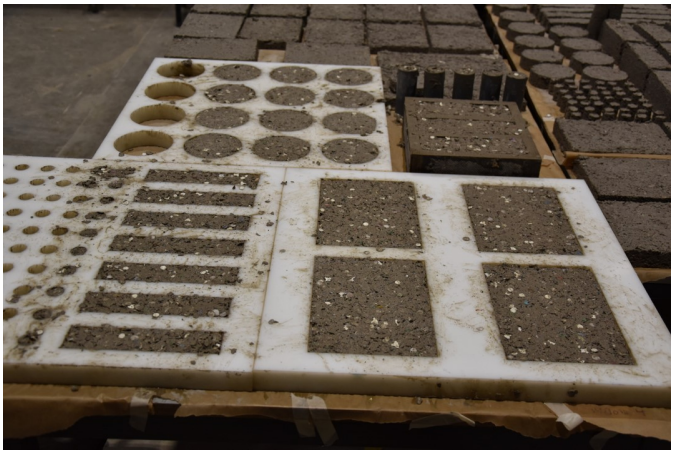

Figure 3.6: Photo taken during molding (picture taken by Mélanie).

Seven different types of sample with different shapes are made, each with different purposes. Indeed, some shapes are more convenient for some kind of tests. The different shapes obtained are illustrated in figure 3.7.

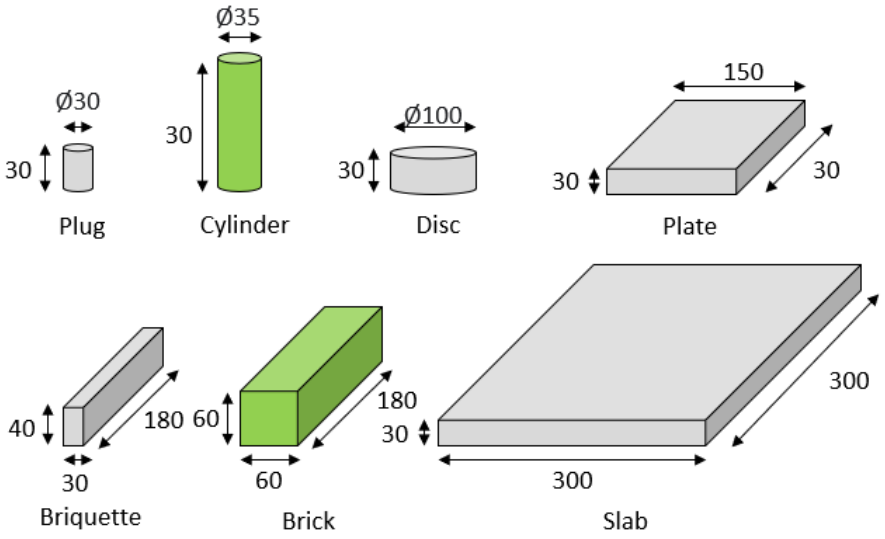

Figure 3.7: Different bricks molded. The dimensions are in [mm].

Since this is a manual operation, some importance is placed on having only one person assigned to the molding of one type of form so that the batch is compressed as uniformly as possible. It is important to note that the molding process is done layer by layer, with manual compression applied between all layers to achieve a compacted material. The samples are finally removed from the molds.

For each composition and for each sample form, some back-up samples are provided, until the material of one composition is completely used (see figure 3.17). The best samples (those with the fewest visual fractures, holes, stones, etc.) are then used in priority for laboratory testing. The shapes of interest in the context of this thesis are drawn in green in figure 3.7 and are the 60x60x180mm bricks and the 35x100mm cylinders. Bricks are used to obtain compression and flexion results in the first campaign, while cylinders are cut out (see section 3.4.3) in order to be adapted for tomography in the second campaign. Other types of shapes are used by Alexis and Eloise in other laboratory tests.

3.2 Variable parameters

Throughout the entire project, we played with the material characteristics, hoping to find the optimal one. Therefore, some variable parameters are defined and tested in different compounds. The following variable parameters are tested:

1. Paper: Three different types of paper are tested as shown in figure 3.8: a "confetti" (10x10mm), a medium band (5x35mm) and a large band (5x290mm). The aim of this analysis is to understand how the material structure and how the distribution in the material will evolve depending on the type of fibre. It is also important to note that the confetti's are a bit harder than the medium and large paper bands.

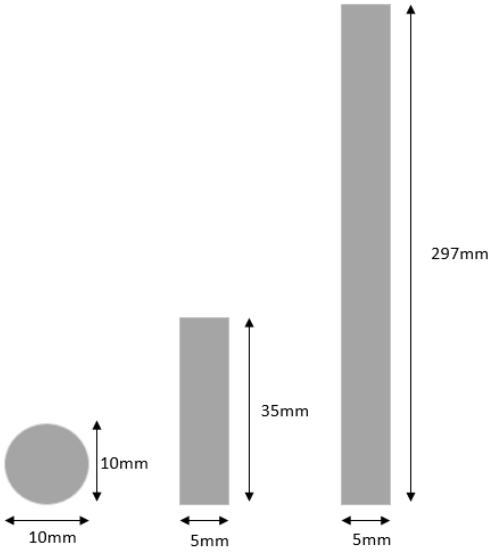

Figure 3.8: Three different types of paper fibers: small (confetti), medium and large.

2. Sand: River sand and crushed sand are tested. Indeed, they have different properties and granulate sizes which affect the properties of the material.

3. Mass proportions of paper: For dry paper, composites composed of 15, 30 and 50% by mass of dry paper are tested. More than 50% is already demonstrated with too low mechanical properties in Mélanie's thesis [11].

4. Mass ratio of sand/lime: 50/50 and 60/40 sand/lime mass ratios will be tested. A certain amount of lime is necessary to hold the mix together because

lime (matrix) is acting as a binder.

5. Mixing time: Results of the first campaign showed that a 6-minute mixing time was more favourable than a 2-minute one. For the second campaign, a shorter time of 5 minutes was compared to a longer mixing time of 15 minutes.

6. Addition of water: When mixing, a little water is added to obtain the reaction of hydraulic lime. Indeed, Hydraulic lime hardens partly by reaction with water (as shown in section 3.1.1) and so differs from other types of lime which harden only by chemical reaction with carbon dioxide present in the air.

In order to know the optimal parameters for our final model, a strategy of varying a single parameter between two compositions is applied. Table 3.2 represents the reference parameters that will be used to carry out our tests.

Variable parameter	Initial measure
Type of paper	Long bands
Proportion of paper	30%
Type of sand	Crushed sand
Proportion sand/lime	50/50
Mixing time	15 minutes
Addition of water	1,25 L/kg
Soaking time of paper	24 hours

Table 3.2: Table of referential parameters.

Testing each combination of characteristics gives a huge variety of samples, and not everything is achievable in one academic year. Therefore, it is important to eliminate some combinations as soon as possible. By changing a single parameter between two samples and analysing the results, a hypothesis can be made. The best parameter is then reused for subsequent samples. By doing this for all parameters, the number of possible combinations of variables is reduced, and an optimal composite is found. Hence, the order of testing must be thought out beforehand to avoid wasting material by making unnecessary samples.

Two test campaigns were designed:
During the *first campaign*, **the soaking time of paper in water** and the **mixing time** are the variable parameters. Different methods are tested to determine how the paper should be soaked:
1) Incorporating the water little by little like a "risotto".

2) Soaking the paper completely in water for one day (24 hours).

And for the mixing time, a short (2 min) and a longer (6 min) mixing time are tested. Differences in the material properties of the compositions are then analysed.

During the *second campaign*, 15 different compounds were initially planned, as shown in figure 3.9. However, based on the results of the first four experiments, some compositions are replaced or removed. Table 3.16 resumes all experiments that were made during the second campaign.

Composition	Papier			Sable		Chaux	Proportions de papier			Rapport sable/chaux		Temps de malaxage		Eau	Dénomination
	petit (confettis)	moyen (35x5mm)	long (290x5mm)	jaune	concassé	hydraulique	15% (40%)	30% (60%)	50% (80%)	50/50	60/40	court (5min)	long (15 min)	commentaire	
	P	M	L	J	C	H	15	30	50	1/1	3/2	5'	15'	E	
1	■				■	■				■			■		P15_C1/1H_15'
2	■				■	■				■			■		P30_C1/1H_15'
3	■				■	■				■			■		P50_C1/1H_15'
4		■			■	■				■			■		M15_C1/1H_15'
5		■			■	■				■			■		M30_C1/1H_15'
6		■			■	■				■			■		M50_C1/1H_15'
7			■		■	■				■			■		L15_C1/1H_15'
8			■		■	■				■			■		L30_C1/1H_15'
9			■		■	■				■			■		L50_C1/1H_15'
10			■	■		■				■					L30_J1/1H_15'
11			■	■		■				■					L30_J1/1H_5'
12			■		■	■					■				L30_C3/2H_15'
13			■		■	■					■				L30_C3/2H_5'
14			■		■	■				■					L30_C1/1H_5'
15 (test)	■				■	■				■			■	Ajout d'eau	P30_C1/1H_15'_E

Figure 3.9: Table of different compounds initially planned in the second campaign (table made by Mélanie).

3.3 First campaign

3.3.1 Samples, parameters and processes

The objective of this campaign is to determine the best solutions for the following two parameters: soaking time of paper in water and duration of mixing. During this campaign, a simple mortar mixer was used. The mixing is driven manually.

The parameters tested are:

1. Soaking time of paper in water: Two different methods are tested: The first method is based on incorporating the water little by little into the mix. More water is added into the mix when the previous quantity is completely merged, like

a "risotto". The samples made by this composition are defined with a "1" (ex: 1TC, 1TL).
The second method consists of soaking paper for one day (24 hours) in a water basin, as shown in figure 3.3. Samples made by this composition are defined with a "2" (ex: 2TC, 2TL). The proportion of water in both experiments is equal, since the water absorbed by the second method is calculated, and additional water is then added during mixing to have equal amounts of water in the final molded compounds.

2. Mixing time: a shorter (2 min) and a longer (6 min) mixing time are tested. The two different times were not defined beforehand, but well during mixing. The shorter mixing time is measured when the water has completely emerged from the mixture (no visible water left, 2 minutes). Samples made with this composition are defined by "TC" (ex: 1TC, 2TC). The longer mixing time is measured when a visual difference appears in the mixture (more shredded paper strips, and a more uniform distribution, 6 minutes). Samples made with this composition are defined by "TL" (ex: 1TL, 2TL).

Finally, four different combinations (1TC, 1TL, 2TC, 2TL, see figure 3.10) are made in order to determine the best combination of variable parameters. The differences between the compositions are represented in table 3.3.

Composition	Risotto	24h soaking	2min mixing	6min mixing
1 TC		X	X	
1 TL		X		X
2 TC	X		X	
2 TL	X			X

Table 3.3: Recapitulating table of compositions for campaign 1.

Medium fibres (the intermediate dimension) with a dry mass proportion of 30% are used, as well as crushed sand and lime in equal mass proportions as shown in table 3.4 and 3.5. At least four bricks of 60x60x180mm are made for each composition (Some have a fifth sample due to leftovers).

The samples are then molded, and the mass of the samples is measured directly after demolding, and a second time after one month of drying at room temperature. The weight of water absorbed by the samples is thus known. The next step is the laboratory testing in order to obtain the stress-strain curves of the four different composites, and to compare the influence of the different parameters.

Element	%	Quantity [kg]
Paper (M)	30	1.2
Lime	35	1.6
Sand	35	1.6
Water		5

Table 3.4: Table of quantity for first mix

Element	%	Quantity [kg]
Paper (M)	30	1.2
Lime	35	1.6
Sand	35	1.6
Water for complete soaking		15
Absorbed water by fibers		3.8

Table 3.5: Table of quantity for second mix

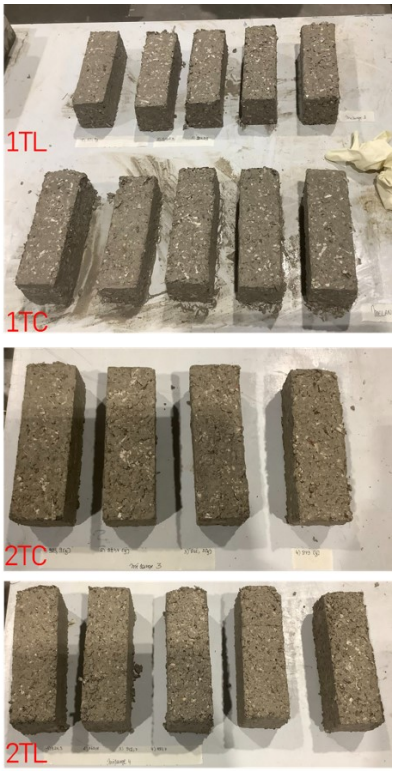

Figure 3.10: First campaign bricks (picture made by Eloise).

3.3.2 Mechanical tests

1. Bending test:
The first flexion tests performed were 3-point flexion tests. In fact, the 4-point flexion test should have been better. Indeed, a 3-point bending is harder to interpret and in 4-point bending, we have a constant moment between the inner supports. The tests are done using a ZWICK brand traction/compression machine with a maximum capacity of 50 kN. The samples used are bricks of 180x60x60mm. The test is performed with a speed of 2 mm/min and an initial distance of 60 mm between supports. Some small wooden bars were installed between the supports and the material, in order to distribute the force (see figure 3.11a). After measuring the samples, the test is carried out until the specimen breaks. The result measures are: the displacement of the crosshead [mm], the force applied in [N] and the test time [s]. The data is transferred to an Excel file. It is then possible to obtain a stress-strain curve and quantify the tensile strength as well as the ductility of the samples.

2. Compression test:
The machine used for these tests is a 100 kN MTS hydraulic press with two fixed plates. The speed is set at 2 mm/min. The samples used are the same as for the bending test. However, since they were broken in half during the bending tests, samples of approximately 90x60x60mm are tested. The initial distance is equal to the height of the samples and is 60 mm. Small metal squares were installed between the supports and the material, in order to distribute the force (see figure 3.11b). The machine measures the applied force [N], the duration of the test [s] and the displacement of the extensometers [mm].

(a) **(b)**

Figure 3.11: a) Bending and b) compression tests (pictures taken by Mélanie).

3.3.3 Results

Bending tests

1. Results

Three samples of each combination of variables were tested. The results are plotted in figure 3.12. Figure 3.12a represents the compositions made by wetting the paper in the mixture like a risotto, while figure 3.12b represent the compositions made with a 24-hour paper soaking time beforehand. The blue curves are the results of the mixed compositions of short duration (2 minutes), while the green curves are the results of the 6 minutes mixed compositions.

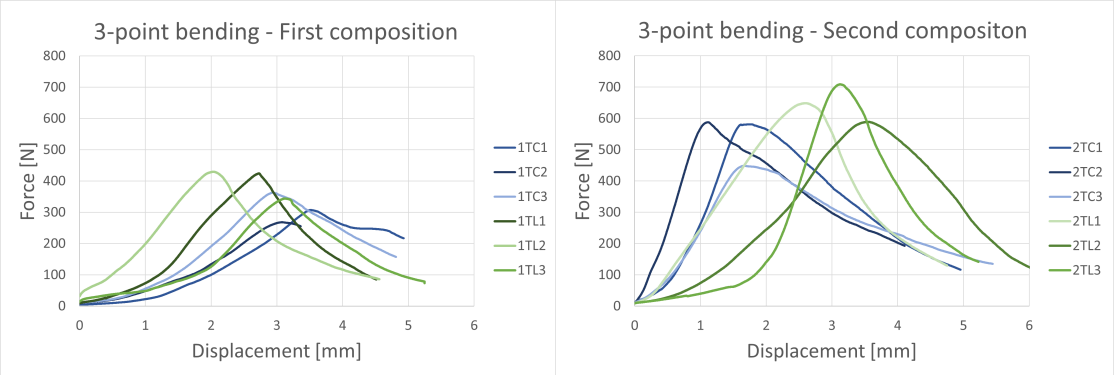

(a) **(b)**

Figure 3.12: Results of the bending tests. Figure (a): Composition made by risotto; Figure (b): Composition made by soaking paper.

2. Interpretation

A difference is noticed: indeed, the strength of the curves from compositions made by soaking paper reaches are much higher than those made by the risotto method. A better comparison is made in figure 3.13. Indeed, the tensile strength is up to 2 times better for the samples from the second composition. This can be explained by the better degradation of paper in the mix. This technique is, therefore, more interesting and is used for all samples of the second campaign. One can also note a difference between the samples made with a low mixing time and with a long one. Indeed, the samples mixed for a longer time reach better bending strengths before fracture.

Compression tests

1. Results

The three samples per composition used for the bending tests were reused for compression tests. However, as each sample is broken in the middle due to the

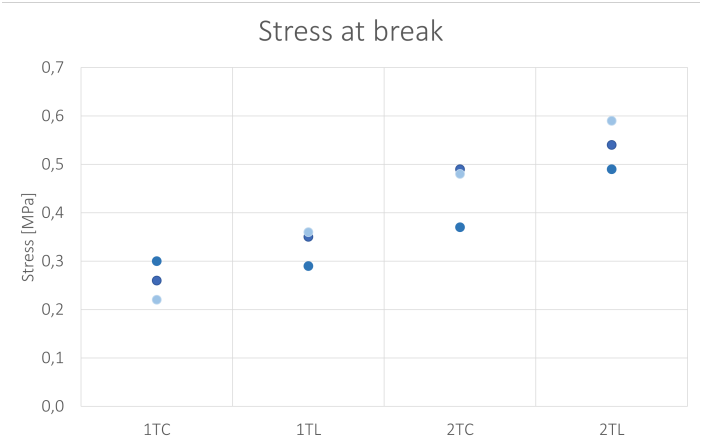

Figure 3.13: Tensile strength of the four different compositions tested.

bending test, 6 samples of each composition are tested. The results are shown in figure 3.14 for each composition. A better view of the different permanent deformation stresses is represented in figure 3.15.

2. Interpretation
Once again, we can notice that there are significant differences between the composites. The composites made by "risotto" are more or less 2 times less resistant than composites made by the second method. The longer mixed samples also achieve higher compressive strengths. This is surely due to the better dispersion and distribution of each component in the material. The conclusion is that solutions made by very little mixing (2 min) are eliminated, and longer times will be tested in the second campaign.

3. Conclusion
In conclusion, both the method of soaking the paper in water beforehand plus a longer mixing time parameter are kept for the future campaigns.

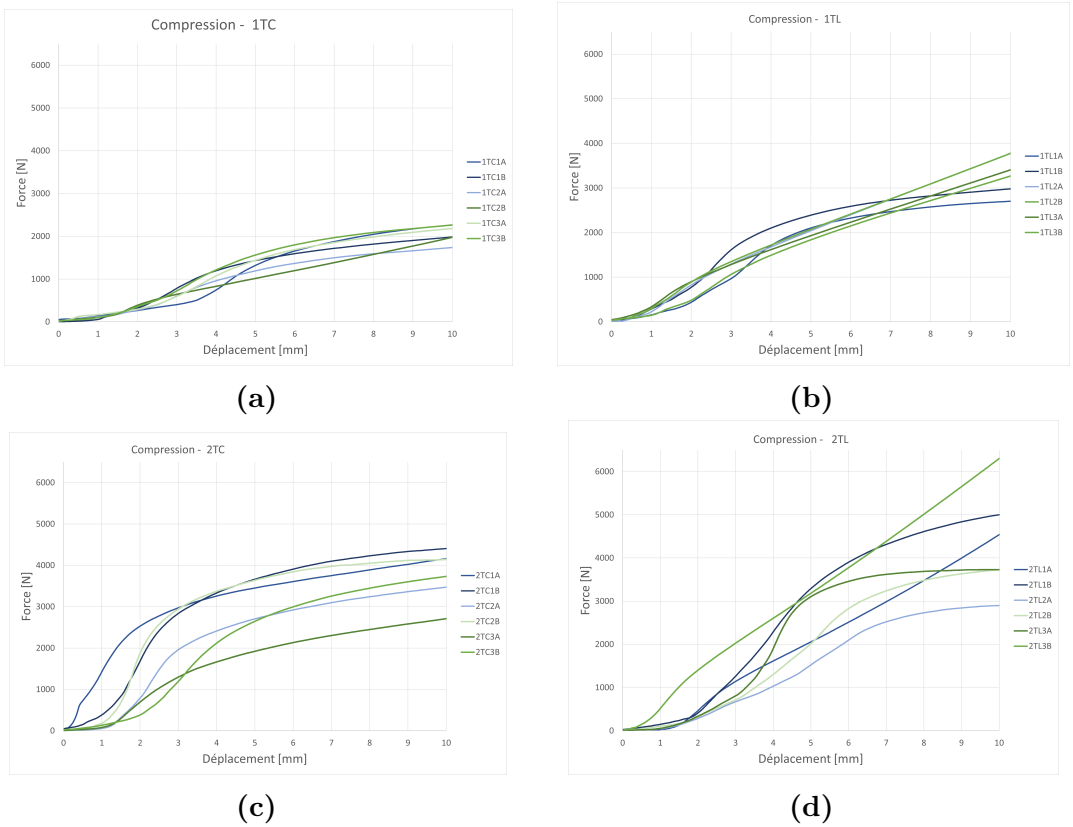

Figure 3.14: Compression differences between different compositions. 3.14a: 1TC (risotto and short mixing); 3.14a: 1TC (risotto and long mixing); 3.14c: 2TC (paper soaking and short mixing); 3.14a: 2TL (paper soaking and long mixing).

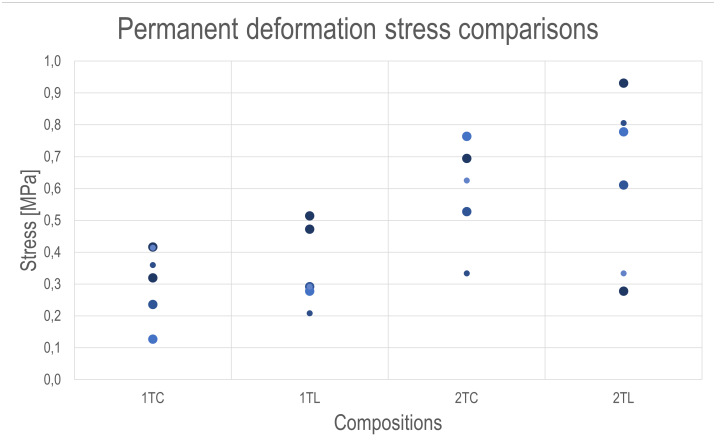

Figure 3.15: Resistance force for 10mm compression.

3.4 Second campaign

3.4.1 Nomenclature

During the second campaign, all the compositions in table 3.16 are produced and tested. The laboratory tests were made by Alexis and Eloïse.

However, not all samples could be analysed by tomography due to a lack of time. Therefore, the most promising compositions or those most interesting for microstructural analysis only are sent for tomographic analysis. The composites analysed are regrouped in table 3.6. Some shortcuts are used to simplify the characterisation of the samples during the rest of this thesis. All samples have a specific modification compared to the sample of reference (REF). The reference composition is made with the parameters found in table 3.2.

Code	Shortcut	Specificity
L30-C1-1H-15	REF	Reference composition.
L30-C1-1H-5-(1)	L-5-1	5 minutes mixing.
L30-C1-1H-5-(2)	L-5-2	5 minutes mixing and 48h soaking of paper.
P30-C1-1H-15	P	Confetti's.
P30-C1-1H-15E	P-E	Confetti's and addition of water during process.
L30-C1-1H-15-(R50)	R50	Composition with 50% recycled material.
L15_C1-1H-15	L15	Only 15 % of paper.

Table 3.6: Table of composites made during the second campaign

3.4.2 Variable parameters

During the second campaign, 15 different compositions have been imagined in order to find the optimal parameters (see figure 3.9). The parameters tested are:

- Type of paper (confetti's / long bands).
- Proportion of paper (15% / 30%).
- Ratio of sand/lime (50 / 50 or 60 / 40).
- Type of sand (River sand / Crushed sand).
- Mixing time (5 / 15 minutes).
- Addition of water (yes/no).

CODE	DATE	COMPOSITION								MIXING TIME	Other	
		Paper size [% dry]			Sand [%]		Ratio	Lime [%]	Time	Comments		
Code composition	Date of molding	small (P)	Middle (M)	Long (L)	Yellow sand (J)	Crushed sand (C)	sand / lime	Lime	[min]	Réf.	Comments
P30-C1-1H-15-(E)	16-12-21	30	0	0	0	35	1-1	35	15	E	Addition of water during mixing
P30-C1-1H-15	16-12-21	30	0	0	0	35	1-1	35	15		
L30-C1-1H-5-(1)	15-12-21	0	0	30	0	35	1-1	35	5	1	
L30-C1-1H-5-(2)	16-12-21	0	0	30	0	35	1-1	35	5	2	Paper is soaked during 48 hours
L30-C1-1H-15	14-12-21	0	0	30	0	35	1-1	35	15		
L30-J1-1H-15	15-02-22	0	0	30	35	0	1-1	35	15		
L30-C3-2H-15	15-02-22	0	0	30	0	42	3-2	28	15		
L50-C1-1H-15	16-02-22	0	0	50	0	25	1-1	25	15		
M30-C1-1H-15	16-02-22	0	30		0	35	1-1	35	15		
L15-C1-1H-15	22-03-22	0	0	15	0	42.5	1-1	42.5	15		
L30-C1-1H-15-(R50)	23-03-22	0	0	30	0	35	1-1	35	15	R50	50% Recycled material in the mix
L30-C0-1H-15	23-03-22	0	0	30	0	0	0-1	70	15		
L0-C1-1H-5	04-04-22	0	0	0	0	50	1-1	50	5		

Figure 3.16: Table of compositions made during the second campaign.

- Compound made of 50% of recycled material.
- Soaking time (24 / 48 hours).

The first four compositions made are compositions (see figure 3.9): REF; P; P-E and L-5-1. In fact, a "fifth" composition (L-5-2) was created during production. Indeed, L-5 was created in 2 times, the differences being in the soaking time of fibres: in the first composition, the paper was soaked in water for 48 hours, while in the second composition, it was soaked only for 24 hours (initial procedure). Finally, the five compositions molded into different forms can be shown in figure 3.17. These five composites are immediately sent for tomographic analysis. Later, the rest of the compositions were produced. After laboratory tests made by Alexis and Eloïse, two more compositions were chosen for tomographic analysis, due to their surprising results. These two composites are R50 and L15. R50 is made by combining 50% of the reference composition with 50% of the recycled composition. The recycled composition is obtained by breaking bricks made with the reference composition. This composition is chosen because it represents the objective of the material, i.e. an eco-circular material.

Figure 3.17: All four first composition samples made (picture taken by Mélanie).

The comparison between samples is done in several ways: the mechanical tests (4-points flexion, compression, DIC acoustic and thermal conductivity tests) are done by Alexis Mazarweh and Eloïse Denis and is analysed in their thesis. On the other hand, this work tries to understand the results of the laboratory tests by microstructural analysis (see section 4).

3.4.3 Choice of samples to analyse

Unfortunately, the tomograph located in KUL is very demanding. Therefore, not all samples were sent in for tomography, due to the excessively long scanning time for each sample. Consequently, some choices of compositions are made for which 2 (R50 and L15) or 3 (REF, L-5-1, L-5-2, P and P-E) samples are sent for tomography.

For each of these compositions, different samples of different shapes were made. Cylinders (as shown in figure 3.18) are the most convenient samples to be analysed. This is because cylinders are more suitable for in-situ compression testing, due to their symmetrical form. The two preferred cylinders for each composition are chosen for tomography. They are determined by simple visualisation, samples with the least imperfections (holes, cracks, stones, ...) are chosen.

Figure 3.18: Example of samples that are send to the tomograph (picture taken by Mélanie).

However, only small samples (40x40x40mm) can get into the tomograph, due to the size of this last one and due to the highly data-demanding analysis. In order to meet this requirement, the cylinders are cut. Indeed, a cylinder is 35mm of diameter and 100mm of height. Since only 3 samples for each composition are allowed, we decided to cut 2 cylinders per composition, as showed in figure 3.19. A first cut is done at 10mm from each of the extremities of the cylinders, as the extremities are a bit more defective than the centre (due to material loss during demolding). Then, a second cut is done in the very centre of the cylinder in order to have two samples from one cylinder (1.1 and 1.2), and a third one from another cylinder (2.1). The samples are then noted with [composition]-[number of sample] (e.g. sample number 1.1 of composition L15 is noted L15-1.1).

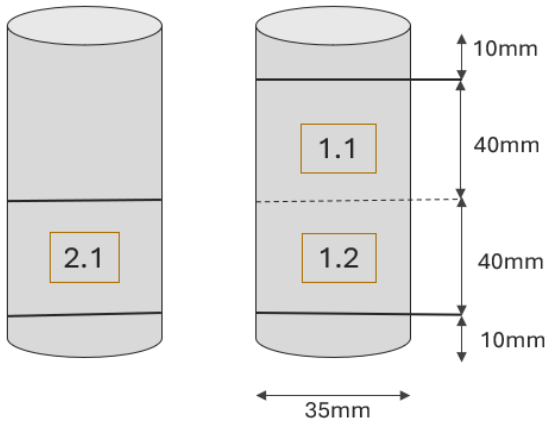

Figure 3.19: Way of cutting the cylinders in 3 samples.

This allows us to compare the difference in distribution and properties between 2 samples from the same cylinder and between two samples from different cylinders. An average will then be done between the three samples to compare compositions between them. Finally, 19 samples were sent and analysed by tomography. Some of the samples of the REF, P, P-E, L-5-1 and L-5-2 compositions represented in figure 3.20 are scanned by the tomograph. All samples are then analysed using the software Aviso.

Figure 3.20: Cylinders for tomography

Chapter 4

Computed tomography analysis

The samples are analysed using the Tescan Unitom XL tomograph, which is installed at the KUL. More than 2500 radiographs were collected for each sample, each being the average of three repeated image acquisitions with an exposure time of 200 milliseconds. The radiograph's data are then inverted into 3D X-ray images using Thermofisher Scientific's software Avizo 3D 2021.1. Each 3D image has a voxel resolution of 20 µm in all directions. The 16-bit monochrome images were saved in Avizo ascii(*am)-format for further processing.

4.1 Image processing and segmentation

The following image processing strategy is adopted:

1. Correction of brightness: The images received are in shades of grey as shown figure 4.1a. The first step is to correct the lack of brightness in all scans. The "convert image type" tool is used. This tool, as its name suggests, allows conversion of the image type as well. Images are then converted from 16-bit to 8-bit monochrome images to win processing time.

2. Volume edit: In figure 4.1b, one can notice that a cylindrical film covers the sample. This film can disturb our results, so it has to be removed. It is done with the tool "volume edit" and by selecting a cylindrical region of interest as shown figure 4.1c. Only voxels inside the cylinder (oriented in the Z axis) are kept, while voxels outside this region are replaced by maximum dark voxels (which are considered like the exterior of the sample).

3. Filtering: In every scan, noise is found (see figure 4.2a). Image noise is a random variation of brightness or color information in images. This noise will

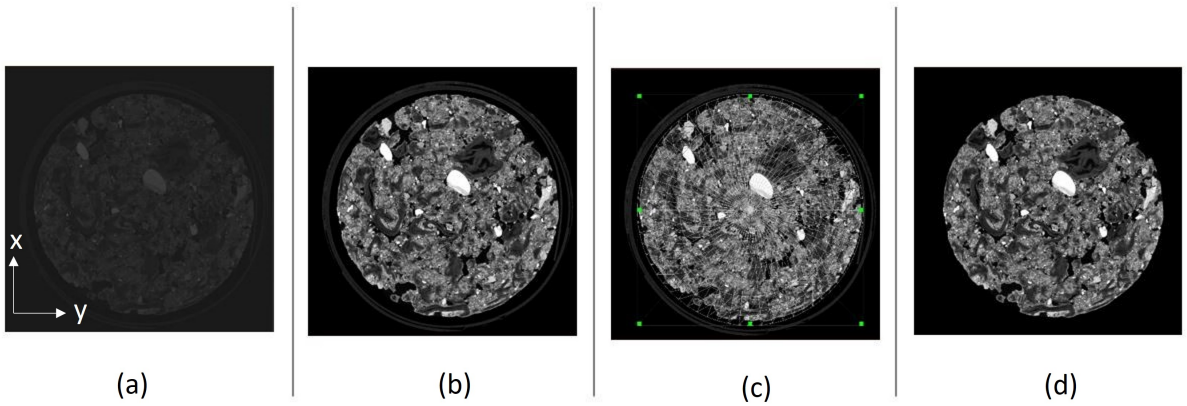

Figure 4.1: Correction of brightness and removing of covering film.

have an impact when calculating volume fractions and must be removed. A 3D median filter with a radius of 26 voxels is then applied to reduce the noise in the images (see appendix A.1 for more information). This step has some benefits: Indeed, noise is reduced and a clear distinction between the different material compounds is made. However, although the noise is removed, some data are incorrect. Indeed, some very small particles (from sand for example) will be replaced by the grey-level of the particles surrounding them. Furthermore, the boundaries between very white voxels and very dark voxels will end up with a grey color, due to average intensity of these voxels. The difference between an unfiltered and a median filtered image in figure 4.2 with data collected from REF-1.1.

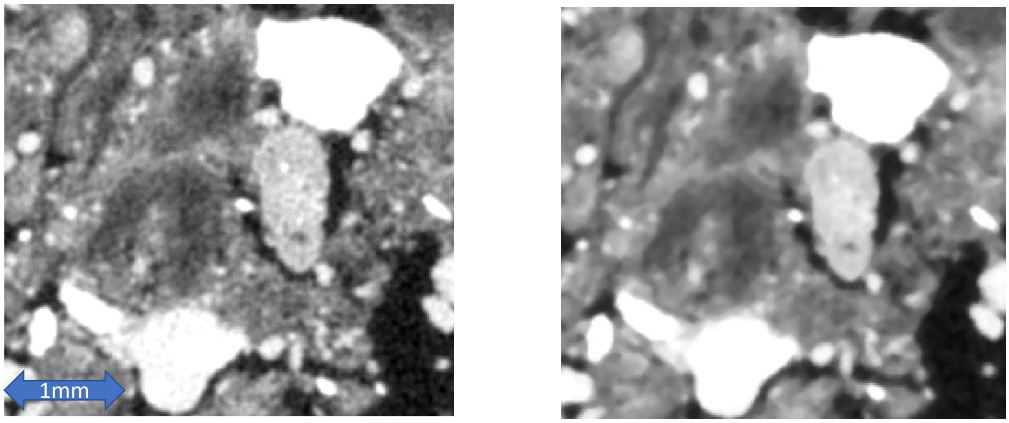

Figure 4.2: Difference between filtered and unfiltered images (REF-1.1). Figure a) is unfiltered, figure b) is filtered.

4. Segmentation: Segmentation of images is a long and very precise step. It is done in the following manner:

1. First of all, it is necessary to separate the air from the material by means of a grey-scale threshold. However, because the samples were relatively dry when they passed through the tomograph, all visible pores in each sample are air-filled. This creates a small challenge: either the air surrounding the samples (exterior) or the pore space inside the samples appears to be dark in the slice images. Knowing the fraction and direction of the pores is essential for the rest of this work, so they must be distinguished from the surrounding air. This is solved by first assigning the "inside" of the material as the regions with grey-scale values greater than or equal to the grey-scale value of paper (which is the least dense material in our composites). By filling in the volume in all scans of our sample, our material with pores included is selected, and a distinction is made between the interior and exterior of the material (see image 4.3).

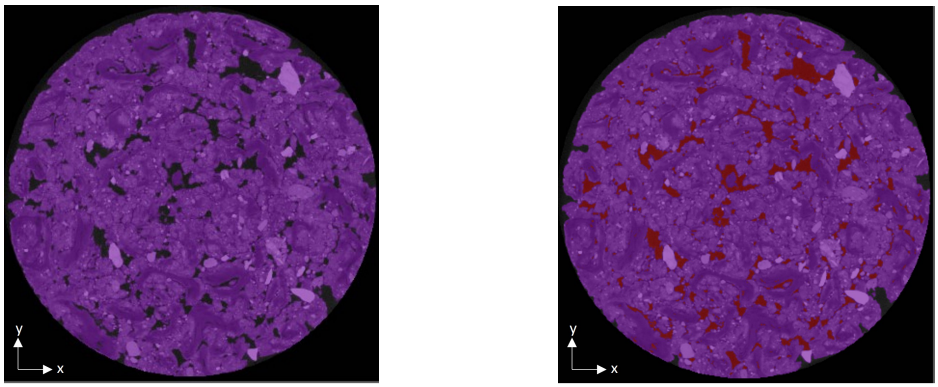

(a) **(b)**

Figure 4.3: Figure (a): before filling; Figure (b): after filling.

2. In the second phase, voxels that correspond to the same component must be separated. All the global thresholding methods available in Avizo 3D are tried in each 3D image to identify a global threshold of grey-scale. We validated the performance of each thresholding approach by visual inspection of three cross-sections, one located between porosity and paper, one between paper and lime and a last one between lime and crushed sand (e.g. image 4.4).

3. Once each fiber has been identified and separated, it is possible to obtain its volume and to identify the position of its barycenter in space as shown for a pore of sample P-1.1 in figure 4.5.

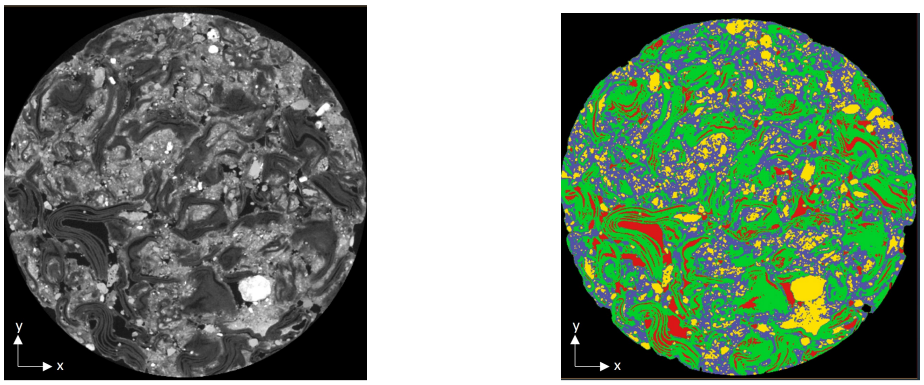

(a) **(b)**

Figure 4.4: Difference between not segmented (a) and segmented (b) images. Red is porosity, green is paper fibers, purple is lime and yellow is crushed sand. Black voxels are the exterior of the sample.

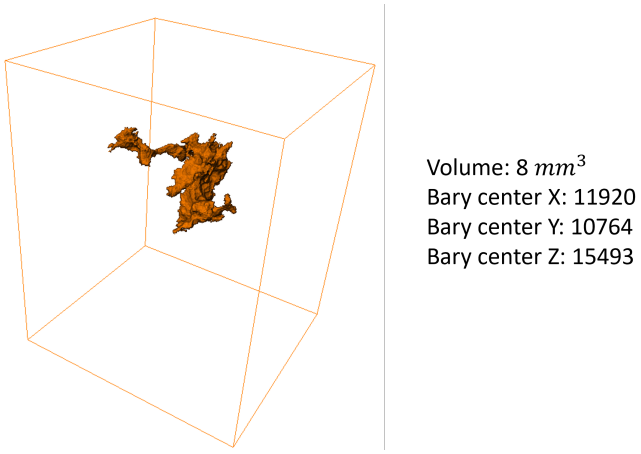

Figure 4.5: Example of data from a pore collected of sample P-1.1.

4.2 Volume fraction

The volume fraction is found for the 19 samples by a simple command called "volume fraction" and by removing the exterior surrounding the sample (black voxels) which is calculated to obtain the real volume fractions of the different constituents.

An experiment is made to check if the theoretical results match to the results received. Indeed, each composite is made with a certain mass proportion of each compound. However, the volume is not calculated. The relation between mass and

volume is :

$$Volume = \frac{Mass}{Density}$$

Thus, the density of each material is necessary to get the theoretical volume fraction. Furthermore, the volume of a compressed compound is not equal to the volume of an uncompressed one. Indeed, in a compressed compound, there are fewer pores, and therefore less volume. The volume fraction received by Avizo separates the pores from the rest of the compounds. Therefore, the aim of the experiment is to find the specific gravity of each compound. Specific gravity is the ratio of the weight of a volume of the substance to the weight of an equal volume of the reference substance. It should not be confused with bulk density which is the weight of a unit volume of a material relative to the same volume of water including voids [6].

To calculate the specific gravity, some water is added to each compressed compound to fill the pores. The mass of the water is measured, and its volume is finally subtracted in the density calculations. It is assumed that the density of water is $1g/cm^3$. Finally, the experiment to get the density of each compound is made following the next steps:

- Dry paper is soaked during 24h (to have the same density of paper as in the second campaign). Hydraulic lime and crushed sand are also prepared.
- The paper, lime and crushed sand are then each put in a different $5000cm^3$ volume bucket. Pressing is not needed as the water will fill the pores (however, paper is pressed to be able to get more fibers in the bucket).
- Water is added until all pores are filled (water is visible at the surface on the top). The mass of the used water is measured.
- The volume of the added water is subtracted to the $5000cm^3$ volume to get the real volume of each compound without pores.
- The specific gravity is deduced by mass/volume.

So, the final equation is (Sg = specific gravity; m = mass of the material component; V = $5000cm^3$; V_w = volume of water):

$$Sg = \frac{m}{V - V_w}$$

4.3 Porosity analysis

The next part is dedicated to the quantitative measurements focusing on the pore system, including the assessment of pore size, shape and spatial distribution. Porosity is present in many materials. Primary porosity is developed through the movement of water due to either absorption into the surrounding masonry unit or evaporation to the air. These pores are highly interconnected and fluid transport through these pores is by capillary transport. Whether it is a defect or a feature, its quantification is crucial. For example, understanding the various types of porosity defects can help adjust the manufacturing process in order to improve the material's properties. Many porosity properties and statistics are calculated, such as volume fraction, sphericity, pore size distribution, pore orientation, anisotropy, and more. Even an attempt of phase correlation between pores and paper is made in appendix E.

4.3.1 Percolation

A question that is of interest in the building sector is the reaction of the bricks with water. During the processing of our material, water is added to the mix. This water could escape through a certain way in the formed samples through gravitational forces, leaving behind traces of her passage. It is then possible that percolation appears in some bricks. Percolation, in physics, chemistry and materials science, refers to the movement and filtering of fluids through porous materials [33]. X-ray computed tomography is frequently used to infer the potential pathways from a 3D representation of the pore network [26]. The aim of the percolation problem in random porous media is to identify the probability at which a connecting pore links two boundaries of the volume. Pores larger than c= 0.3 mm in equivalent cylindrical diameter (henceforth macropores) allow water to bypass the material matrix rapidly [13]. This fast transport of water and other substances that takes place near saturation in well-connected pore networks is called preferential flow [26]. A highly percolating sample would have a form of pores similar to figure 4.6, where one can clearly notice a connection between the upper and the lower sides of the sample along the z-axis.

In the context of this thesis, percolation could lead to a greater tendency for the material to fracture in a certain direction. Therefore, a 3D view of the pores of the system as well as a 3D view of the pores with a volume greater than $2.10^8 \mu m$ (to have a clearer view of the percolating system) is provided. Interconnectivity of the pores are then quantitatively investigated in the samples via X-ray computed tomography.

Figure 4.6: Example of percolating soil [26].

4.3.2 Void orientation

Even if the material is not percolating, porosity is still present in the material in the form of voids. Voids are sites of weaknesses that control the mechanical properties of the materials. Indeed, the porosity formation, which obviously depends on the matrix composition and microstructure, affects significantly the elastic modulus, yield strength, ultimate tensile strength, and ductility [3]. The pore's shapes and sizes can easily be found by tomography with the "arithmetic" tool to isolate the pores from the rest of the material, followed by "labeling" to distinguish each pore from the others, and finally "label analysis" to get a table giving information about each pore (e.g. the Barycenter, the volume, the connectivity, ...). The pores are described with five independent variables: [x, y, z] for location and [ϕ , θ] for orientation as shown in figure 4.8.

A very interesting subject in void topology as well as in crystallography is the isotropic character of the material. This one is known through the orientation and shape of its pores. Indeed, some materials have different hardnesses depending on the direction in which the hardness test was performed. Isotropy means that there is uniformity of the pores in all orientations. Anisotropy means that the properties of the porous medium do not have same values in all directions. This is an interesting topic because in general, anisotropy is caused by periodic layering which is our case. The first measurement of the isotropic character of the pores, is to analyse their sphericity. Sphericity is the measurement of how spherical an object is and is represented by the following formula:

$$Sphericity = \frac{\pi^{1/3}(6V)^{2/3}}{A}$$

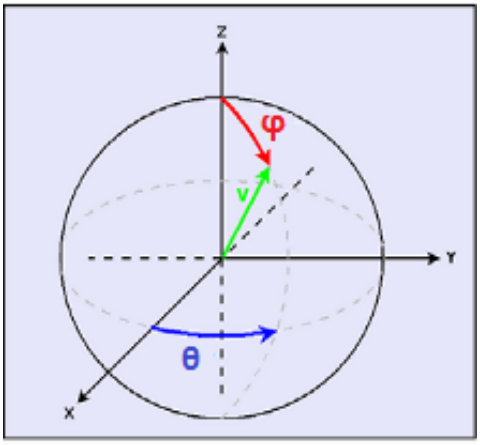

Figure 4.7: Spherical coordinates.

Where V is the volume of a particle, and A is its surface area. The sphericity of a sphere is one, any particle which is none sphere will have a sphericity less than one.

Knowing by segmentation visualisation that the voids are not spherical, the orientation of those is researched. The orientation of the pores is analysed via two methods in the samples:

Method 1: Feret diameter

Feret diameter is defined as the distance between two parallel tangents of a particle in a given direction (see Figure 4.8).

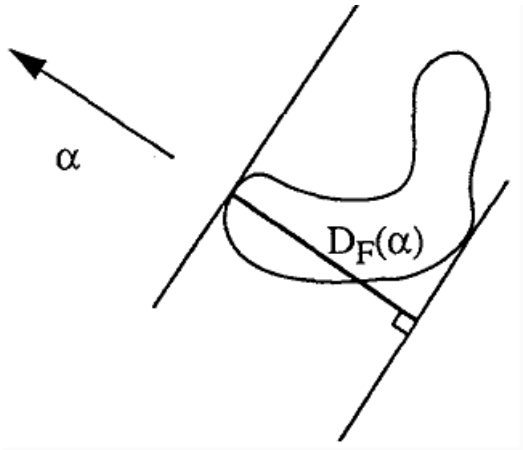

Figure 4.8: Feret diameter in direction α.

This definition is extended to 3D with the distance between two tangent planes. Feret diameters are then computed along all directions [x,y,z]. The orientations are defined by the couple of angles from spherical coordinates. As shown in figure 4.8, angle Φ(in degrees) is between [0,+90]. For each pore, the maximum of the Feret diameters is calculated. An average of the maximum Feret diameter of all pores is also available. Consequently, if the average of the maximum Feret diameters of all pores is near $\phi = 0°$, it means that the pores tend to be parallel to the z axis (and that they were influenced by the gravitational force acting on water during processing). If it is closer to $\phi = 90°$, it means that the pores tend to be parallel to the x-y plane. The Θ angle gives some information about the angle in the x-y plane. This is not interesting in our case, since the material is symmetrical around the z axis, and no interest has been made for the correct placement of the sample around this axis. The minimum of the Feret diameters is also calculated, in order to know if there is a least preferred orientation.

Method 2 : Inertial moment

Inertial moments are also used to observe the tendency of the pores in a certain direction. Therefore, the centroid or center of mass of each pore must be found. The first order moments will define the centroid of each pore.

$$M_{1x} = \frac{1}{A(X)} \int_X x dx dy dz$$

$$M_{1y} = \frac{1}{A(X)} \int_X y dx dy dz$$

$$M_{1z} = \frac{1}{A(X)} \int_X z dx dy dz$$

The inertial moment matrix is then calculated around those centroids with the components of the matrix defined with following formula's:

$$M_{2xy} = \frac{1}{A(X)} \int_X (x_i - M_{1x})(y_j - M_{1y}) dx dy dz$$

The covariance matrix is then established:

$$\begin{bmatrix} M_{2xx} & M_{2xy} & M_{2xz} \\ M_{2yx} & M_{2yy} & M_{2yz} \\ M_{2zx} & M_{2zy} & M_{2zz} \end{bmatrix}$$

Again, two orientations are calculated:

1. The maximum inertial moment is defined as the direction of its major inertia axis. It is given as the eigenvector of the largest eigenvalue of the inertia matrix. The orientation is defined as for the Feret diameter in figure 4.8, with results of ϕ-angle between 0 and 90 degrees.

2. The minimum inertial moment is defined as the direction of its minor inertia axis.

The preferential orientation of the pores is then inferred.

Finally, the degree of anisotropy is calculated. This is the measure of the deviation of the pores from the spherical shape. It is calculated with the following formula:

$$Degree\ of\ anisotropy = 1 - \left(\frac{smallest\ eigenvalue}{largest\ eigenvalue}\right)\ of\ the\ covariance\ matrix$$

The closest the values of the smallest and largest eigenvalues are, the less the anisotropic character there is. Indeed, maximum and minimum eigenvalues equality means that there is no privileged structural direction. The degree of Anisotropy is 0 for perfect isotropy and 1 for complete anisotropy.

4.3.3 Size of voids

Two values are fundamental to describe porous materials, and are calculated:

- **Total Porosity (TP)** is defined as the fraction of the total volume that is occupied by pores. An increase of total porosity is an indication of decreased compressive strength. This would also influence the critical tensile strength. The total porosity is measured by computed tomography and is already done in section 5.2).

- **Pore Size Distribution (PSD)** is defined as the fraction of total pore volume in which the pores lie within a stated size range. Pore Size Distribution would indicate if the gain in total porosity represents a coarsening of pores or an increase in the amount of pores. In most damage cases the increase is due to an increase in pore size. The pore size distribution is computed in the form of a histogram.

Different types of pores are identified and classified in three categories in function of the diameter of the pores: Macroporosities (greater than 50nm diameter), Mesoporosities (2-20nm diameter) and Microporosities (less than 2nm diameter) as shown in figure 4.9. However, the data from tomography is precise to 9 μm and

therefore only macropores are identified. [29]. Macropores are mainly separated in capillary pores and coarse pores. Capillary porosity (0.01–100 μ m) plays a major role for mechanical properties (compressive strength). Coarse pores are larger pores and are generally formed by entrapped air. They are irregular in shape and distribution and can account for up to 8% total porosity [29]. They form through the entrapment of air during the mixing process.

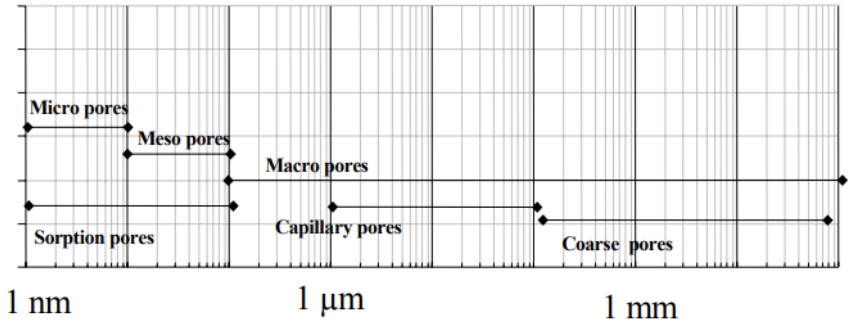

Figure 4.9: Characterisation of porosity.

4.4 In-situ compression

This part aims to use X ray tomography for studying the mechanical behaviour of structural materials through in-situ experiments. The question that is tried to be answered here is: could a compression step be useful during the creation of the material ? Indeed the mechanical treatment of mortars such as compression can reduce the entrained air content near the surface by pressing the air out. The tomograph used for the in-situ tests is a Deben CT5000 stage. Each 3D image scan has a voxel resolution of 30 µm in all directions. In-situ compression imaging is time and data storage intensive. Indeed, all scans must be given for every moment of compression. Therefore, the compression of a single sample of each composition is analysed in computed tomography. For each composition, the cleanest of the previously analysed samples is chosen. This is the one that seems to have the least number of defects (e.g. a starting fracture in the sample, a big stone in the center, a hole made when demolding, a not uniform distribution). The selected samples are L-5-1-1.2; L-5-2-1.2; REF-2.1; P-1.2; P-E-2.1; R50-1.1; L15-1.1.

4.4.1 Graphical analysis

When testing the brick great care must be taken, as the paper-brick never failed catastrophically, it is simply compressed like squeezing rubber. The data received (the force at each instant [N], the deformation [mm] and the time [s]) by the tomograph is saved as an excel-file. The maximum stress before plastic deformation is also computed and compared for the different compositions. The stress is calculated as the ratio of the force [F] on the air (A=πr^2) of the sample:

$$\sigma = \frac{F}{A}$$

4.4.2 Image segmentation analysis

Images at more than 25 moments during the compression are collected and analysed for each sample with Aviso. An important parameter obtained by treating this data is the compressibility. Isothermal compressibility is defined as:

$$\beta_T = -\frac{1}{V}\frac{\delta V}{\delta p}$$

where V is volume and p is pressure. The volumes of the samples are calculated before and after compression by image segmentation analysis. However, the metal clamps put on the samples (see figure 4.10) to have a better dispersion of the force, need to be removed beforehand by image processing.

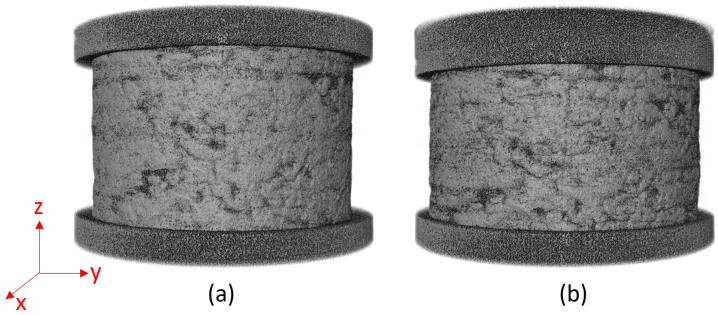

Figure 4.10: Example of initial and final 3D view of REF sample.

It is important to note that the final volume analysed is from compressed samples (stress is still applied on the samples). Therefore, there is no elastic deformation noticeable, after relaxing the pressure. It should be noted that the 35x40 cylinders will not have uniaxial compression (there will be stresses towards other directions than the axis). Indeed, when we have a very flat object, there is a lot of friction. During compression, the material tries to expand laterally to keep its volume but due to the friction with the plate, the material in contact with the plates cannot expand laterally. To compensate these stresses appear, and there is no longer uniaxial compression. This phenomenon is called the barrel effect (the fact that the material does not expand in contact with the plate but more in the center). This is not a problem for the calculations, you just have to know it.

4.4.3 DVC analysis

Finally, a Digital volume correlation (DVC) local approach is performed on the REF-composition sample. DVC is a technique to compute 3D full-field continuous displacement and strain maps from volume images acquired during a deformation process of an object. This module can for instance be used to visualise and quantify deformation-induced microstructural changes during dynamic processes. For example, a result that could be expected is represented in figure 4.11. One can see the barrel effect in this figure, with low compaction levels represented in blue, and large compaction levels in red.

However, obtaining such data in tomography analysis required better adapted samples, as cylinders of 35x40mm are too rich in $30\mu m$ voxels, and therefore can not be analysed in good conditions. Re-sampling the samples through image processing is not a sufficient solution, as the samples still are too big. Nevertheless, an attempt of DVC local analysis on sample REF-1.2 is made.

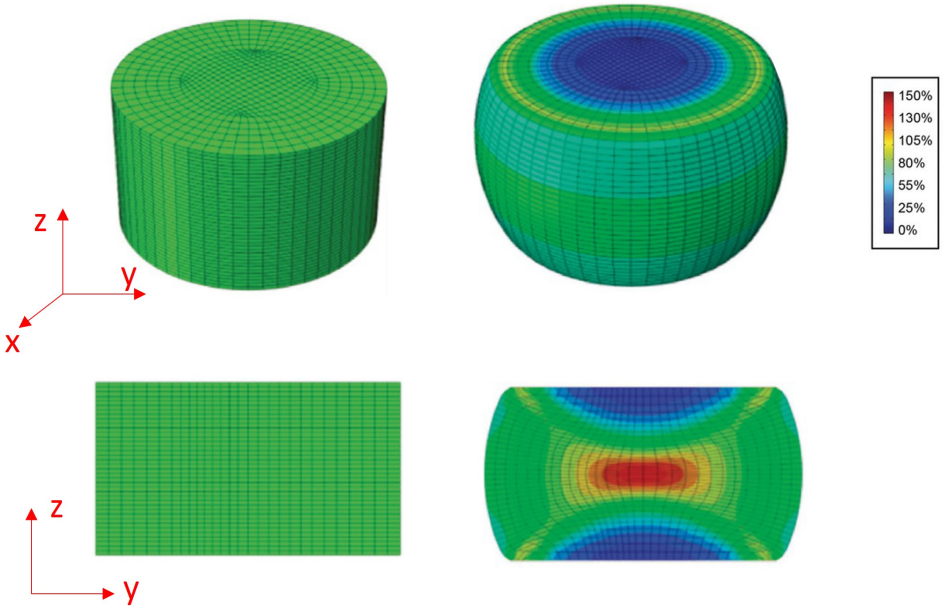

Figure 4.11: Example of Digital Volume Correlation representing the barrel effect [7].

Chapter 5

Results

5.1 Segmentation

1. Results
A representation of a XY-plan resulting from each individual sample can be found in appendix B. In each scan, porosity is represented in red, paper in green, lime in purple and crushed sand in yellow. Figure 5.1 gives a first insight of the microstructures of the different compositions. In order to make a visual comparison between compositions, a single scan representative of the microstructure of each composition is kept. It is important to note that not all scans presented are always representative of the volume fraction in the composites. Indeed, the representation of a scan is chosen here among more than 2500 scans, and there is some dispersion of volume fractions between scans. The volume fraction in each sample is calculated in section 5.2.

2. Interpretation:
The three different samples of the same composition are compared together. After some visual analysis between all scans of all samples, there are no obvious differences between the three samples of the same composition. Indeed, the same microstructure is observed overall in all the samples of the same composition. There are no clear visual characteristics of compounds that could have been more compressed or whatsoever. However, some samples are more defective than others. For example, it is clearly observed in figure 5.2 that composition P-C1.2 has large yellow stones within the material. These stones are from the crushed sand. Some samples also have more pores clustered in the center (see P-1.1 in figure 5.2) or at the corner of the material, or even large paper pellets inside. All these defects will surely impact the properties of the material, with possible cracks appearing near these defects.

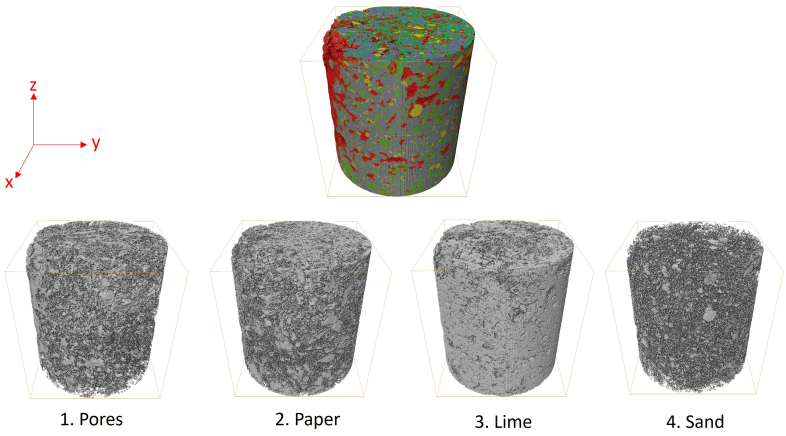

Figure 5.1: 3D view of segmentation of sample REF-1.2. Red is porosity, green is paper, purple is hydraulic lime and yellow is crushed sand.

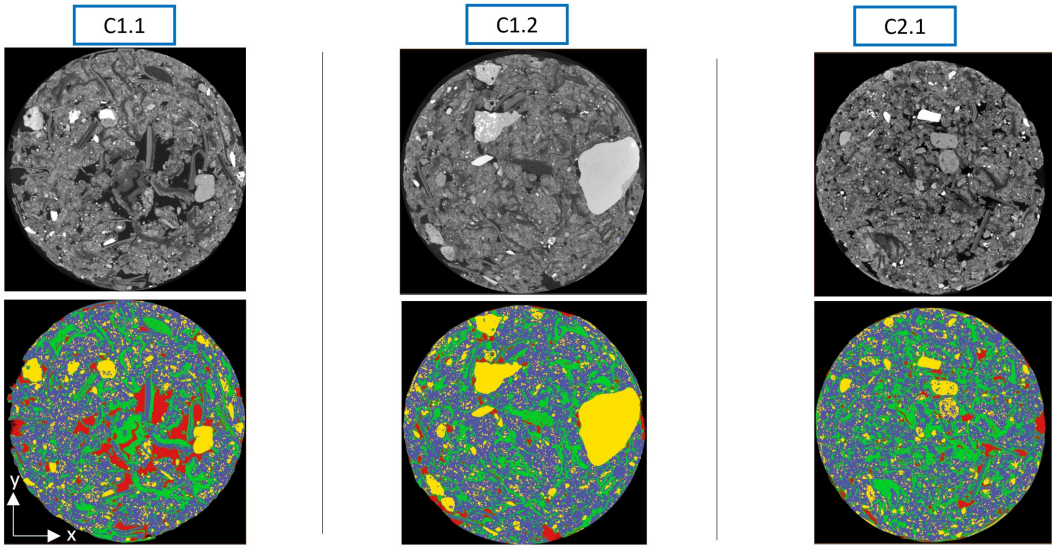

Figure 5.2: XY-plan scan of segmentation of the three samples of P. Red is porosity, green is paper, purple is hydraulic lime and yellow is crushed sand.

The objective now is to find differences and similarities between the different compositions, first by visual analysis of their microstructure. Some representative images of the different compositions are put here below. In all scans: red is porosity, green is paper, purple is hydraulic lime and yellow is crushed sand.

1. Differences between L-5-1 and L-5-2:
The processing difference between L-5-1 and L-5-2 is the **soaking time of the paper** in the water basin. Indeed, the paper of composition L-5-1 is soaked for 24 hours in water, while 48h for composition L-5-2. The results are found in figure 5.3. Some similarities between these compositions can be noticed: The mixture is not so well distributed: Indeed, the paper forms some pellets or long filaments. Furthermore, the pores are mainly found inside these paper pellets. No clear difference can be made between these two compositions, as they are very visually similar.

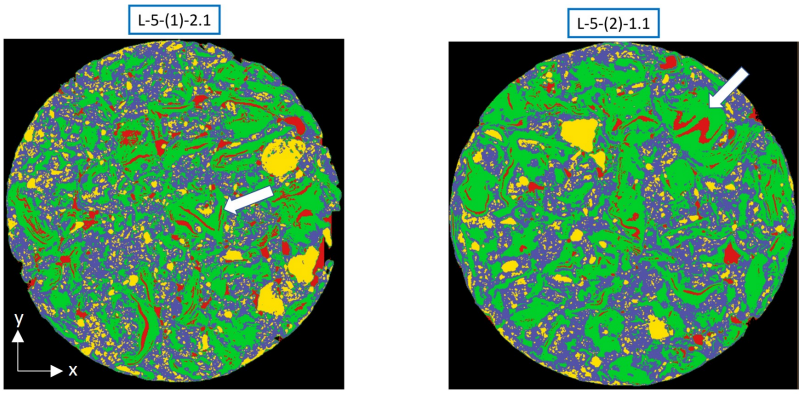

Figure 5.3: XY-plan scan comparison between composition L-5-1 and L-5-2.

2. Differences between L-5-1 and REF:
The second comparison is between L-5-1 and REF. The changing parameter here is the **mixing time**. It can be noticed in figure 5.4 that there are fewer paper pellets and long filaments in the reference composition, but paper is still found in the form of filaments. The material is already much more distributed. It can be observed that the pores are no longer located inside the paper pellets anymore, as they are broken. However, the pores are still located near to paper bands.

3. Differences between REF and P:
The third comparison is between REF and P composition, as shown in figure 5.5. The changing parameter here is the **size of the paper bands**. Indeed, the REF composition is made of long paper bands, while the P composition is made of confettis. In both images, paper is still found in the form of filaments but

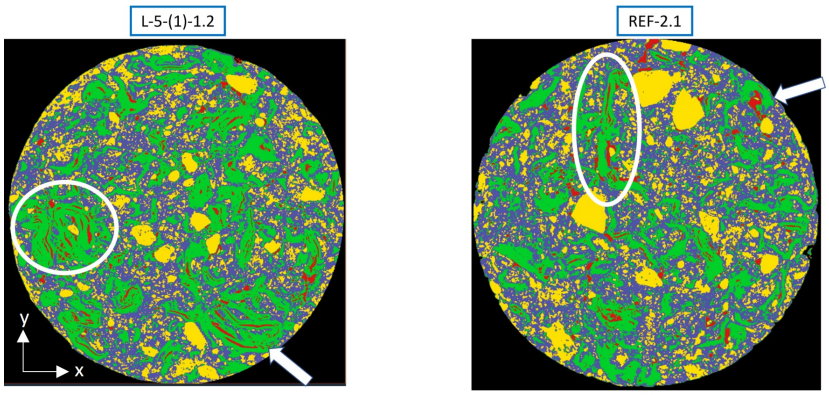

Figure 5.4: XY-plan scan comparison between composition L-5-1 and REF.

there are fewer for the composition made of confettis. One can also observe that in composition P the pores are almost not located inside the filaments of paper anymore. Moreover, the appearance of "lines", a linear structure, is noticed in composition P.

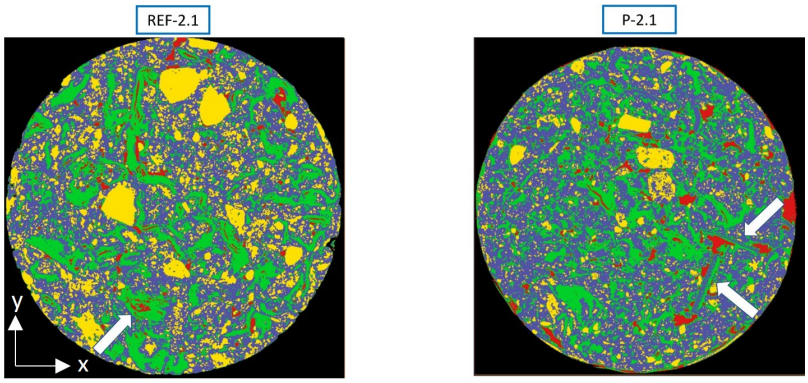

Figure 5.5: XY-plan scan comparison between composition REF and P.

4. Differences between P and P-E:
The fourth comparison involves the P and P-E composition, as shown in figure 5.6. The changing parameter here is the **addition of water during mixing**. A clear difference appears: Indeed, a linear structure is found for composition P-E, while a mainly random structure is found for composition P.

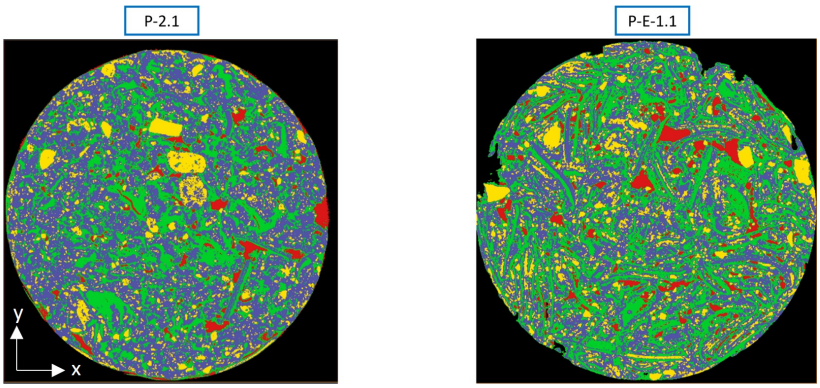

Figure 5.6: XY-plan scan comparison between composition P and P-E.

5. Differences between REF and R50:
The comparison between composition REF and L15, is represented in figure 5.7. Composition R50 is composed of 50% of REF and **50% of recycled REF**. There is no clear visual difference between both compositions.

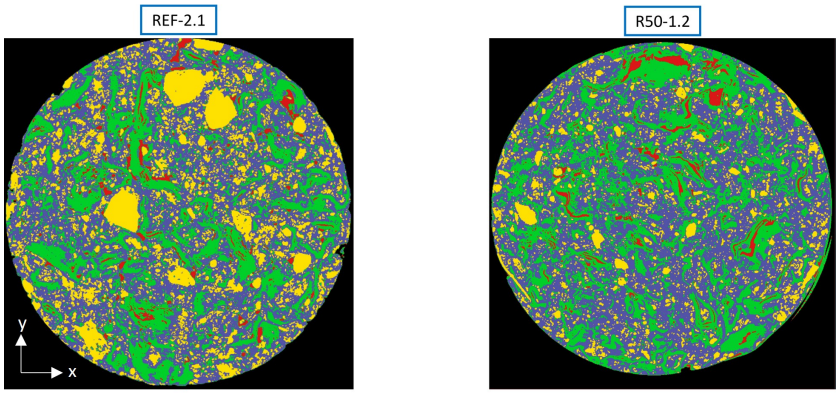

Figure 5.7: XY-plan scan comparison between composition REF and R50.

6. Differences between REF and L15:
The comparison between composition REF and L15, is represented in figure 5.8. The changing parameter here is the **proportion of paper**. Indeed, composition REF is made with 30% paper bands, while composition P is made with 15% paper bands. Of course, there is a clear difference in proportions. Under the microscope, it can be observed that the paper filaments of composition L15 are finer. Indeed, less paper pellets are made. Therefore, there is a better distribution of the paper along the material.

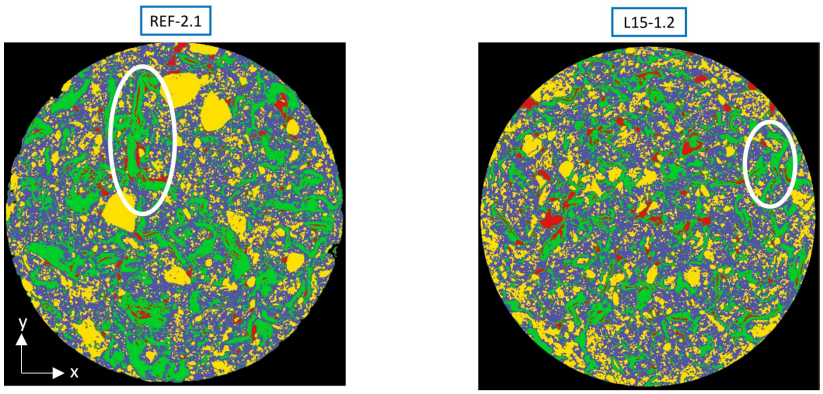

Figure 5.8: XY-plan scan comparison between composition REF and L15.

3. Conclusion

Finally, table 5.1 lists the main visual microscopic differences observed due to the changing parameters. Furthermore, all scans shown have some similarities. Indeed, on all scans, paper is found in form of linear filaments, with pores around it (see phase correlation between the pores and the paper in appendix E). Indeed, pores are sometimes interpolated in paper pellets/filaments or sometimes bonded to the boundary of paper fibers. Another observation is that lime is interconnected in all compositions. Indeed, one can draw a line from one side of a scan to the other side, by passing exclusively on lime (and this for all compositions). Crushed sand however, is always interpolated in the matrix (lime), and is represented by grains of all sizes. A phase correlation analysis between hydraulic lime and crushed sand by checking the possible chemical between those two components can be interesting to execute in the future.

Parameter	Effect of variable parameter compared to REF composition.
Soaking time (24/48h)	- No clear distinction between compositions can be made.
Duration of mix (5/15min)	- More paper-pellets are found. - More incorporated voids inside the paper fibers. - Worse distribution of the material compounds.
Size of paper fibers (small/long)	- Shorter paper filaments. - Pores are not incorporated in paper filaments. - Linear structure.
Addition of water (yes/no)	- Appearance of a complete linear structure.
50% Recycled material (yes/no)	- No clear distinction between compositions.
Proportion of paper (15/30%)	- Smaller and thinner filaments of paper are observed. - No paper pellets.

Table 5.1: Summary table after visual inspection of the microstructural analysis.

5.2 Volume fraction

1. Results:
The volume fraction results for each sample are noted in appendix C. Since each of the samples of a composition has more or less similar values, an average of the 3 samples of each composition is taken. The average of each composition is represented in table 5.2. These values are then compared in figure 5.9.

	Porosity [%]	Paper [%]	Lime [%]	Sand [%]
REF	8	33	45	14
L-5-1	5	39	41	15
L-5-2	6	42	39	13
P	7	29	52	12
P-E	9	35	42	15
R50	6	28	49	18
L15	9	19	51	22

Table 5.2: Table of average volume fraction obtained for each composition.

Besides, specific gravity of each material compound is determined by experimental test, with calculations in appendix C.1. To make 100 samples, the volume and volume fraction of each materials component that should be obtained are represented

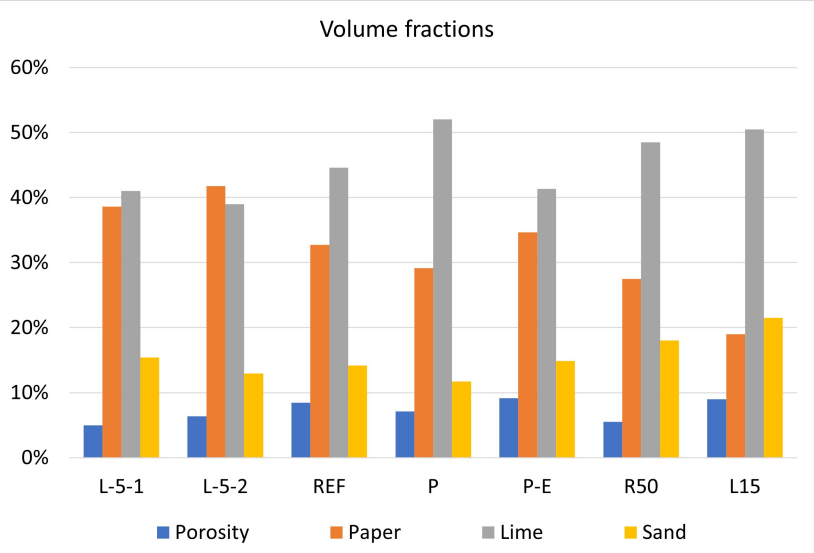

Figure 5.9: Comparative graph of volume fraction for the different compositions.

in table 5.3.

	Specific gravity	Weight	Volume $[cm^3]$	volume fraction [%]
Paper	1.1	4200	3747	43
Sand	2.8	5600	1993	23
Lime	2	5600	2856	34

Table 5.3: Volume fraction obtained by experimental measures

2. Interpretation
When comparing the results from image analysis with the one resulting from experimental tests, there is a volume fraction difference up to $\pm 10\%$ for each material compound. There is a clear distinction for sand. Indeed, lower values are obtained for sand by imaging analysis than by experimental measurements. Assumptions are made to explain this difference:

- The main possible reason is that there is a proportion of materials with almost the same specific gravity as lime (e.g. ceramic and lime itself) in crushed sand. These are then of the same grey-level as the hydraulic lime and are then accounted for as lime by image analysis.
- Secondly, during image processing, a median filter is used to reduce the noise. However, some data is inevitably transformed during this step. Indeed, small

grains of sand and fine paper fibers are transformed into their neighbourhood. Lime being the matrix, it is mostly the neighbour of these particles, and earns some voxels during filtering.

- It is very difficult to find a perfect threshold between components during the segmentation step. Indeed, the limit between lime and sand for example is not always clear to see with shades of grey. The determination of the thresholds between components is best done by simple visualisation.
- Finally, only a small portion (3 samples) of the material is analysed. More than 100 samples were made for each composite and it is therefore possible that the 3 chosen samples have different distributions than the rest of the composite, due to the smaller proportion.

3. Conclusions:
To conclude, lime is the most common material compound found by image analysis with average proportions varying between 39 and 52 %. This volume fraction is higher than the volume fraction found by experimental measures because of all the reasons discussed before. The second most spread material is paper with average values between 28 and 42% (19% for L15). Composition L-5-1 and L-5-2 have the highest paper volume fractions, and the lowest lime volume fraction. The sand reaches volume fraction values between 12 and 18% (22% for L15) and the porosity of the material is between 5 and 9%. Porosity is measured as the void spaces in the material, and is a fraction of the volume of voids over the total volume. This value is very low, compared to most rocks and soils (see table 5.4).

Material	Porosity [%]
Paper brick	5-9
Sandly soil	36-43
Surface soil	20
Hydraulic lime	15
Cement mortars	25
Bentonite	9
Bentonite+ sand	6

Table 5.4: Porosity in different materials. Bentonite is a type of rock.

5.3 Porosity analysis

5.3.1 Percolation

1. Results:
A 3D view of the pores of each composition is shown in figure 5.10. Each color corresponds to a different pore.

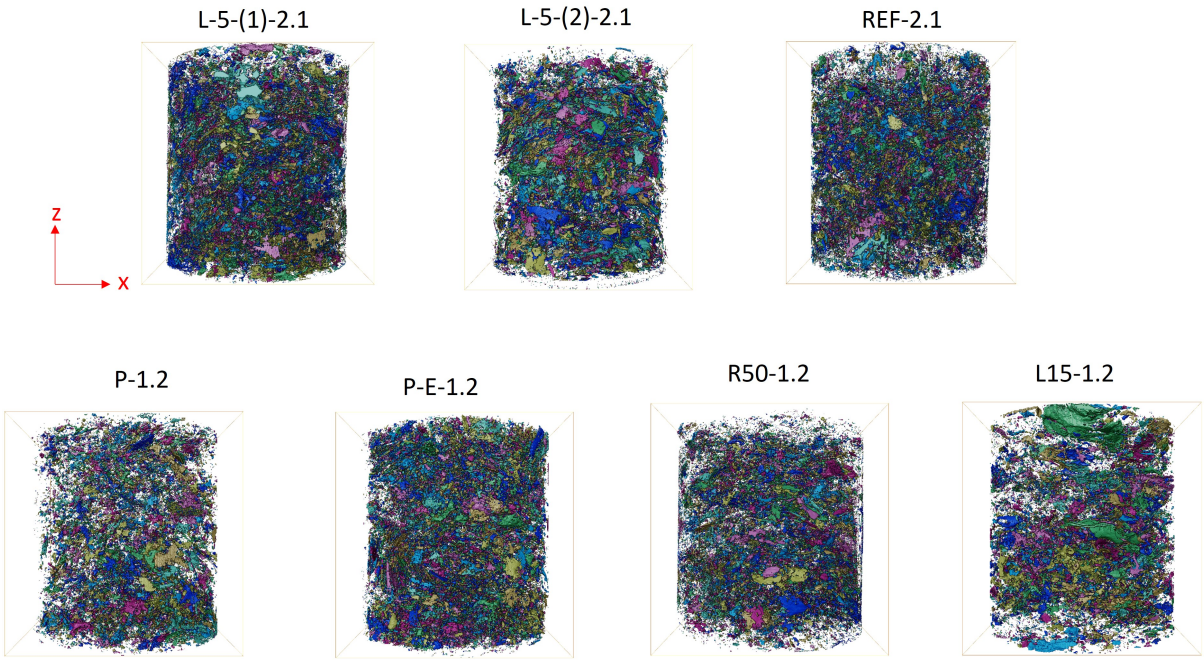

Figure 5.10: 3D view of the porosity of the different compositions. Each color represents a different void.

However, one cannot know through this image if there is a pore inside connecting both extremities of the sample. Therefore, a filter is applied keeping only pores with a volume larger than $10^6 \mu m^3$ (see figure 5.11).

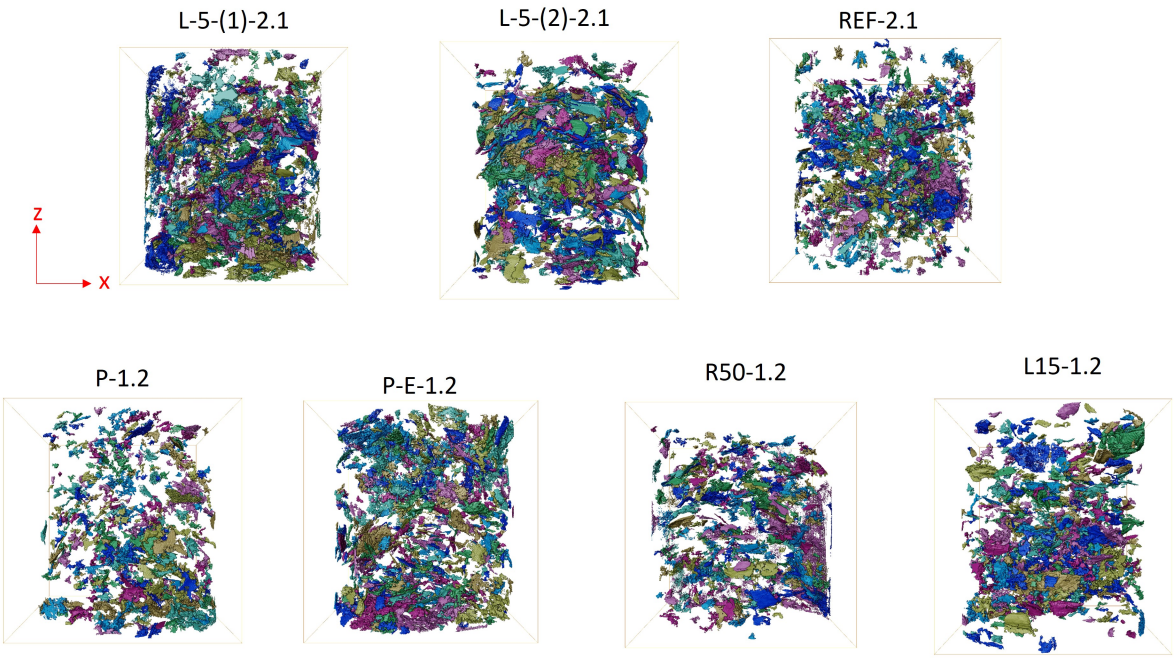

Figure 5.11: 3D view of the porosity of the different compositions with a filter $10^6 \mu m^3$. Each color represents a different void.

2. Interpretations:
By simple visualisation of the 3D porosity with this second filter, it can already be deduced that there is no obvious percolation in any of the samples (as in figure 4.6). Indeed, two extremities of a sample are not interconnected. Furthermore, there is no clear tendency of the pores to elongate in the z-axis direction.

3. Conclusions:
The material is not percolating, and there is no interconnectivity between pores. The gravitational forces acting on water during the drying process does not seem to have a huge impact on the material.

5.3.2 Void orientation

1. Results:
The orientation of the average maximum and minimum Feret diameters of the pores of the different samples and their average volume are represented in table D.1. The average of all different compositions is represented below in table 5.5.

	Max. Feret diameter [°]	Min. Feret diameter[°]	Max. inertial moment[°]	Min. inertial moment[°]
L-5-(1)	58	55	58	57
L-5-(2)	56	53	59	57
REF	57	54	59	58
P	57	53	59	58
P-E	58	52	59	56
R50	59	54	59	56
L15	61	50	62	52

Table 5.5: Table of average Feret and Inertial moments orientations for capillary and coarse pores.

When a filter of volume greater than $10^6 \mu m^3$ is applied to obtain data exclusively for coarse pores, table D.2 in appendix D is obtained, and the average for each composition is represented in table 5.6.

	Max. Feret diameter [°]	Min. Feret diameter[°]	Max. inertial moment[°]	Min. inertial moment[°]
L-5-(1)	70	38	69	38
L-5-(2)	71	38	72	38
REF	70	39	71	38
P	71	37	72	38
P-E	70	38	70	39
R50	72	39	71	38
L15	71	40	73	40

Table 5.6: Table of average Feret and Inertial moments orientations for coarse pores.

Finally the sphericity and anisotropy of the pores of the different compositions are represented in table 5.7.

	Sphericity [-]	Anisotropy [-]
L-5-1	0,22	0,83
L-5-2	0,27	0,84
REF	0,40	0,81
P	0,33	0,80
P-E	0,42	0,77
R50	0,31	0,80
L15	0,24	0,82

Table 5.7: Comparative table of sphericity and anisotropy for the different compositions.

2. Interpretations:
For a percolating material, the orientation of the mean of the maximum Feret diameters should be closer to 0°, while the minimum of Feret diameters should be closer to 90°. Here, the average of the maximum of Feret diameters for each sample remains close to 58° and the minimum close to 53°. In the same way, the minimum and maximum orientation computed with the inertial moments are around [58-59°]. It can already be deduced that porosity has a greater tendency to elongate in the x-y plan than in the z axis direction. It is even more clear for coarse pores (in table 5.6). Indeed, the maximum of Feret and inertial moments both show values of 70°, while the minimum of Feret and inertial moment show values around 38°. If the material was percolating, a percolation threshold could have been identified in the composition, with the Feret minimum average used as the diameter of the percolating "tubes". Neither the different treatments nor the different sizes and proportions of the components had a significant effect on the characteristics of the imaged pore.

The pores are also far from being spherical. Indeed, the values of sphericity for the different compositions are between 0,22 and 0,42 (a sphere has a sphericity of 1). Indeed, the pores show a very anisotropic character, with values around 0,8 (a complete anisotropic composition has a value of anisotropy of 1). *3. Conclusions*
Distinction is made between capillary and coarse pores. However, both types of pores are not spherical in all compositions, as they have an anisotropic character. The pores of the different compositions also have a preferred orientation. Indeed, the xy-plan is favoured. It is also much more the case for coarse pores than for capillary pores. This can be explained because the molding process is done layer by layer, with compression steps between layers, which can cause large horizontal pores to exist between them. It is a frequent phenomenon happening with this type of processing. There are no clear differences between compositions.

5.3.3 Size of voids

1. Results:
The Total Porosity is already calculated in 5.2. The total volume and average volume of the voids in each sample are computed and represented in appendix D.1. The average for each composition is represented in table 5.8.

	Total Porosity [%]	Total pores volume $[10^{12}\mu m^3]$	Mean volume $[10^6\mu m^3]$
L-5-1	5	1,9	1,2
L-5-2	6	2,4	2,0
REF	8	3,2	0,9
P	7	2,7	1,5
P-E	9	3,5	1,4
R50	6	2,1	1,3
L15	9	3,5	2,6

Table 5.8: Average volume of the pores for each composition.

The Pore Size Distribution for each composition is represented in figure 5.13. A comparative of the fraction of capillary and coarse pores is represented in table D.3 in the appendix and in figure 5.13.

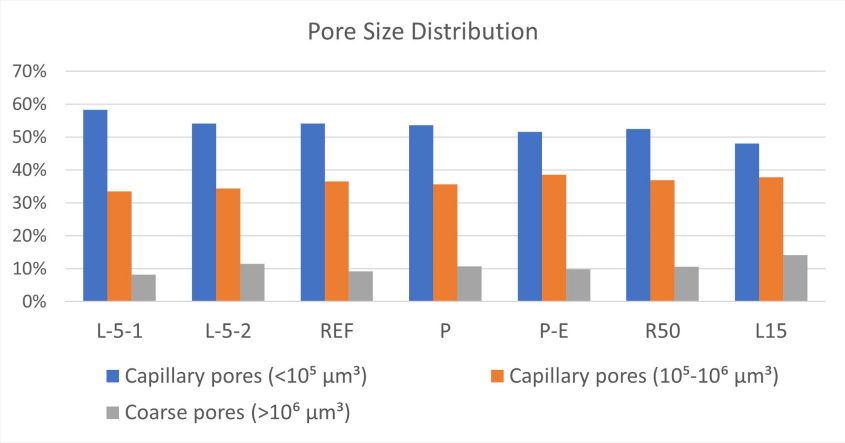

Figure 5.12: Comparative graph of Pore Size distribution for each composition. Composition P-E has the most capillary pores, while composition L15 has the most coarse pores.

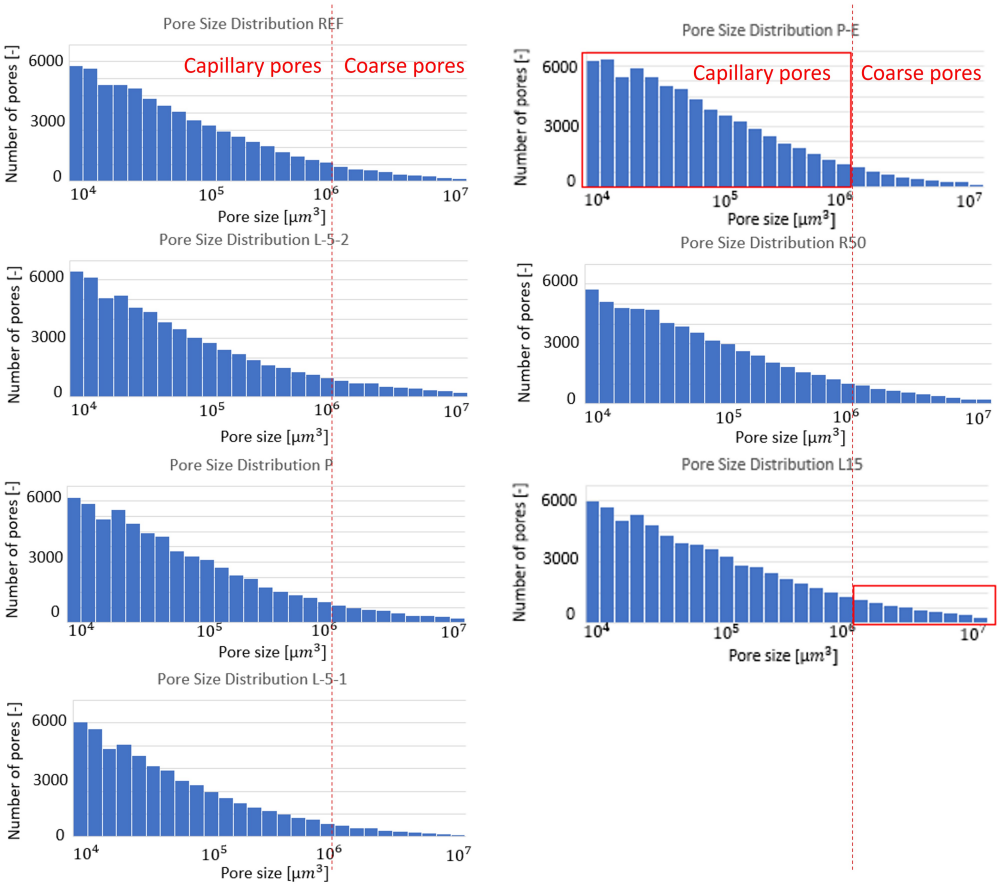

Figure 5.13: Pore Size distribution for each composition. Composition P-E has the most capillary pores, while composition L15 has the most coarse pores.

2. Interpretations:
All compositions have similar values. The level of porosity is really low compared to other construction materials. One can observe in figure 5.13 that composition P-E reaches higher values for large capillary pores ($10^5 - 10^6 \mu m^3$), while composition L15 has a higher fraction of coarse pores($> 10^6 \mu m^3$). Therefore, these two compositions have a higher total porosity than the other compositions. Composition L-5-1 has the smallest total porosity, because the composition has a lower coarse pores fraction.

3. Conclusions:
Pore sizes are similar between all compositions. The difference in total porosity is less than 4%, and the differences in pore size distribution are low (maximum 6% for coarse pores). These differences may have an impact on the material proper-

ties, as the compressive and tensile strength are very dependent on the porosity. Composition P-E is made mostly of capillary pores, which explains its sphericity value larger than other compositions.

5.4 In-situ compression

5.4.1 Graphical analysis

1. Results:
The data received by the in-situ compression is saved as an excel file. The force-displacement curve of the different compositions is shown in figure 5.14), and the maximum stress before permanent deformation of the different compositions is represented in figure 5.15

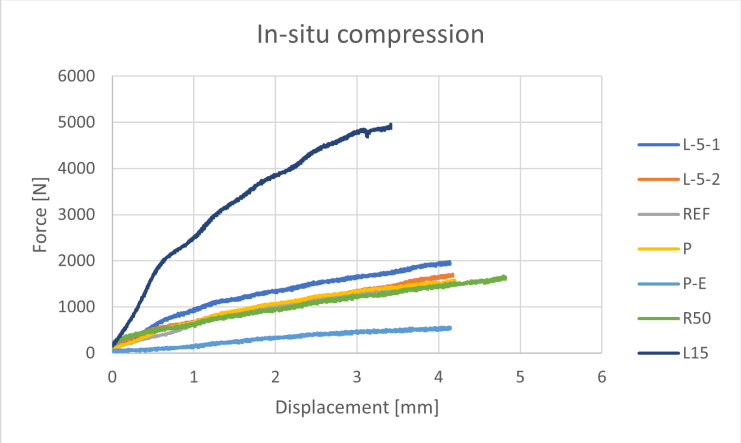

Figure 5.14: Force-displacement graph of the different compositions after in-situ compression test.

2. Interpretations:
The ultimate compressive strength of the materials is not observable in figure 5.14 because the material never fails completely. It is observed in figure 5.15 that composition L15 is more than 2 times stronger than the others, while composition P-E is 2 times less resistant. There are no clear differences between compositions L-5-1, L-5-2, REF, P and R50, as they have similar values.

3. Conclusions:
The only parameters that have a big impact on the compressive strengths are the proportion of paper (better properties with lower proportions of paper) and

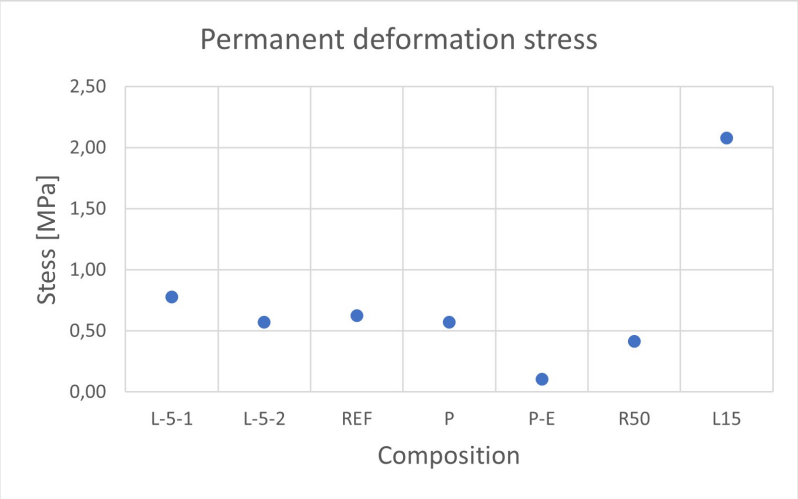

Figure 5.15: Maximum stress before permanent deformation of the different compositions after in-situ compression test.

the addition of water during mixing (lower compressive strength with addition of water). No conclusions are made for the other compounds as only one sample from each composition is tested, and values are quite similar.

5.4.2 Image segmentation analysis

1. Results:
The images resulting from the different samples are found in appendix F. For illustration, figures 5.16a and 5.16b are analysed before compression on sample REF-1.2 and are analysed after compression in figures 5.17a and 5.17b.

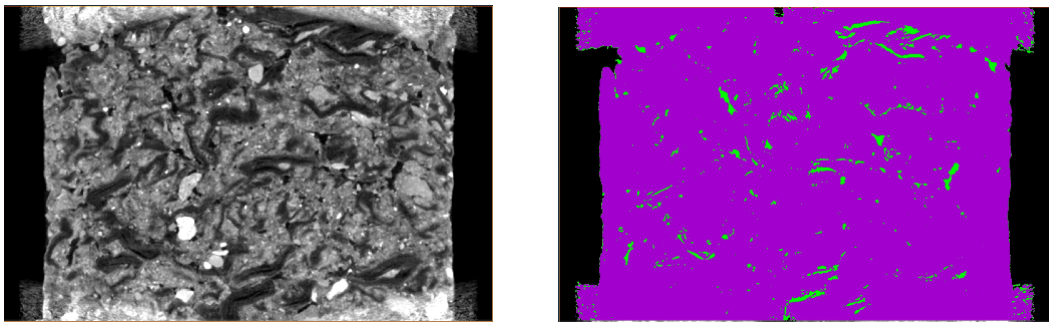

(a) **(b)**

Figure 5.16: Segmentation before in-situ compression. Porosity is represented in green, sand lime and paper in purple.

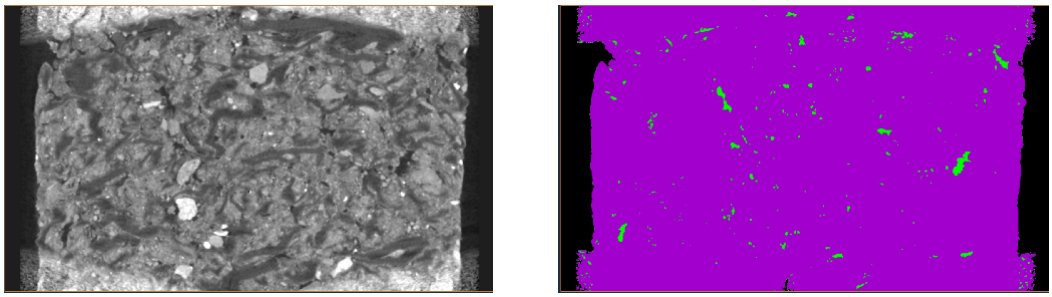

(a) **(b)**

Figure 5.17: Segmentation after in-situ compression. Porosity is represented in green, sand lime and paper in purple.

Table 5.9 is a comparative table of initial and final volume and porosity obtained for each sample. However, this data is not precise: Indeed, the actively scanned volume by the tomograph is smaller due to the field of view defined by the scan resolution and due to presence of the metal clamps on the top and bottom of the samples, which also limit the height that can not be well reconstructed. Therefore, the initial heights measured for all samples have values around 27 mm while it should have values around 40 mm. This is a problem, since compressibility depends on the height of the samples and is the reason why Poisson's ratio is not discussed (more information in appendix F). However, the initial volume and initial porosity of the samples is known in section 5.2). The final volume can then be reconstructed by the following steps:

- Measure the initial (P_I) and final (P_F) porosity of the in-situ scans for each sample.
- The ratio of real final porosity P_{Fr} to the real initial porosity P_{Ir} is equal to the ratio $\frac{P_F}{P_I}$. So, the real final porosity is calculated as $P_{Fr} = P_F \cdot \frac{P_{Ir}}{P_I}$
- The final volume (V_f) is then calculated as: $V_f = V_i(1 - \frac{P_{Fr}}{PIr})$.

The compressibility is then calculated with these measurements and the results are in table 5.10.

	Initial volume $[10^{12}\mu m^3]$	Initial porosity [%]	Final porosity [%]	Final volume $[10^{12}\mu m^3]$
L-5-1	37,2	5	2,6	36,3
L-5-2	38,9	6	5,4	38,6
REF	36,4	8	5,4	35,4
P	37,2	7	4,2	36,2
P-E	37,3	9	4,3	35,5
R50	40,4	6	3,6	39,4
L15	38,1	9	5,4	36,7

Table 5.9: Volume analysis before and after compression.

	δV $[10^{13}\mu m^3]$	δp $[10^6 N/m^2]$	Compressibility $[10^{-8}m^2/N]$
L-5-1	0,9	2,04	1,2
L-5-2	0,3	1,78	4,3
REF	1	1,57	1,8
P	1	1,63	1,6
P-E	1,8	0,56	8,6
R50	1	1,69	1,5
L15	1,4	5,15	0,7

Table 5.10: Comparative table for the compressibility of each composition.

2. Interpretations:
In table 5.9, it is observed that the porosity is decreasing for every composition. Therefore, the total volume is also decreased. It is observed in figure 5.16b and 5.17b that the pores aligned in the XY-(horizontal) plane are completely filled after compression. However, the pores oriented in the z-(vertical) direction are not completely filled. The compressibility of each composition is compared in table 5.10. Composition L15 obtains the lowest compressibility with $7.10^{-9}[\frac{m^2}{N}]$, while composition P-E obtains the highest compressibility.

3. Conclusions:
In conclusion, pores parallel to the xy-plane are mostly filled due to the compression. However, pores aligned in the z-axis are not filled, and are still found in the material after compression. Composition L15 has a lower compressibility than the other materials, while P-E has a higher compressibility.

5.5 DVC analysis

1. Results:
The result of the DVC analysis for sample REF-1.2 is represented in figure 5.18.

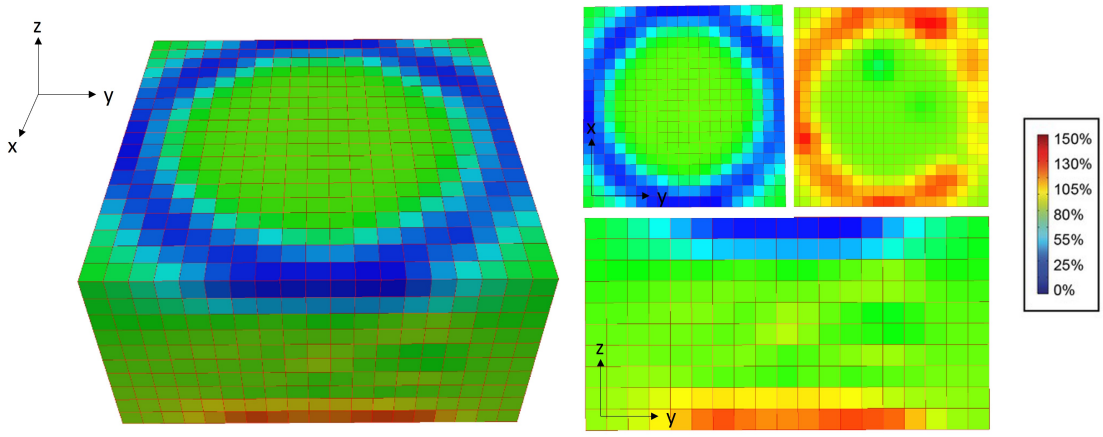

Figure 5.18: DVC results of sample REF-1.2

2. Interpretations:
As the DVC analysis is high-data demanding, a cylinder could not be extracted from the data without re-sampling the materials and creating a new mesh. This step requires cutting the sample at least in half and too much data is then lost. The results are then not representative of the global reaction of the in-situ compression anymore. However, a DVC local analysis is performed on sample REF-1.2 without re-sampling it (figure 5.18).

There are clearly two circles appearing on the north and south side of the sample. The circle on the north side is blue, while the one on the south side is red. The blue voxels are voxels that in the initial state represented the material, but due to the load acting on the material, those voxels are replaced by air after compression, in their final state. The red voxels are voxels that represent the expansion of the material due to the compression, and are therefore more interesting. One can see that the red circle is not uniformly distributed, so there are orientations that are preferred for the expansion of the material. The green voxels at the edges represent exterior air.

3. Conclusion
A DVC analysis is a time and data demanding analysis and requires adapted samples. However, it could be interesting in the future to perform a DVC analysis

on every composition to have a better idea of the movement of every particle in the material at microscopic scale. The fracture initiations happening in the samples can then be identified, and a solution can then be improved to avoid these fracture initiations.

Chapter 6

Discussion

6.1 Link microstructural analysis with laboratory tests

The aim of this section is to understand the laboratory test results made by Eloise and Alexis by analysing the microstructure of the different compositions. Results obtained in chapter 5 are compared with the results of Alexis and Eloïse, that are found in their master's thesis: "Development of a new eco-circular composite material for construction application: SPALCO (2022)". Therefore, most of the graphics represented in this section are resulting from their thesis. The compositions that are analysed in this thesis are framed in red in each graphic.

6.1.1 Segmentation

First of all, let's discuss mechanical properties of the compositions. Figure 6.1a represents the average Young's modulus, figure 6.1b the average compressive strength before fracture, and figure 6.1c represents the average flexural strength for each composition.

L15 has the best mechanical properties. Indeed, its Young's modulus and compressive strength are more than 5 times better than the properties of the reference composition (3 times better flexural strength). This is due to the higher proportion in sand and lime of the composite. Indeed, more sand boost the mechanical strength of the composite (better Young's modulus), and more lime boosts the bonds between the different material compounds. Another reason is that paper in fewer quantity is not creating large paper pellets as we can find in the reference composition. Indeed, as each material compound reacts differently to a specific compressive load, some defects can appear, which can create fractures. For example,

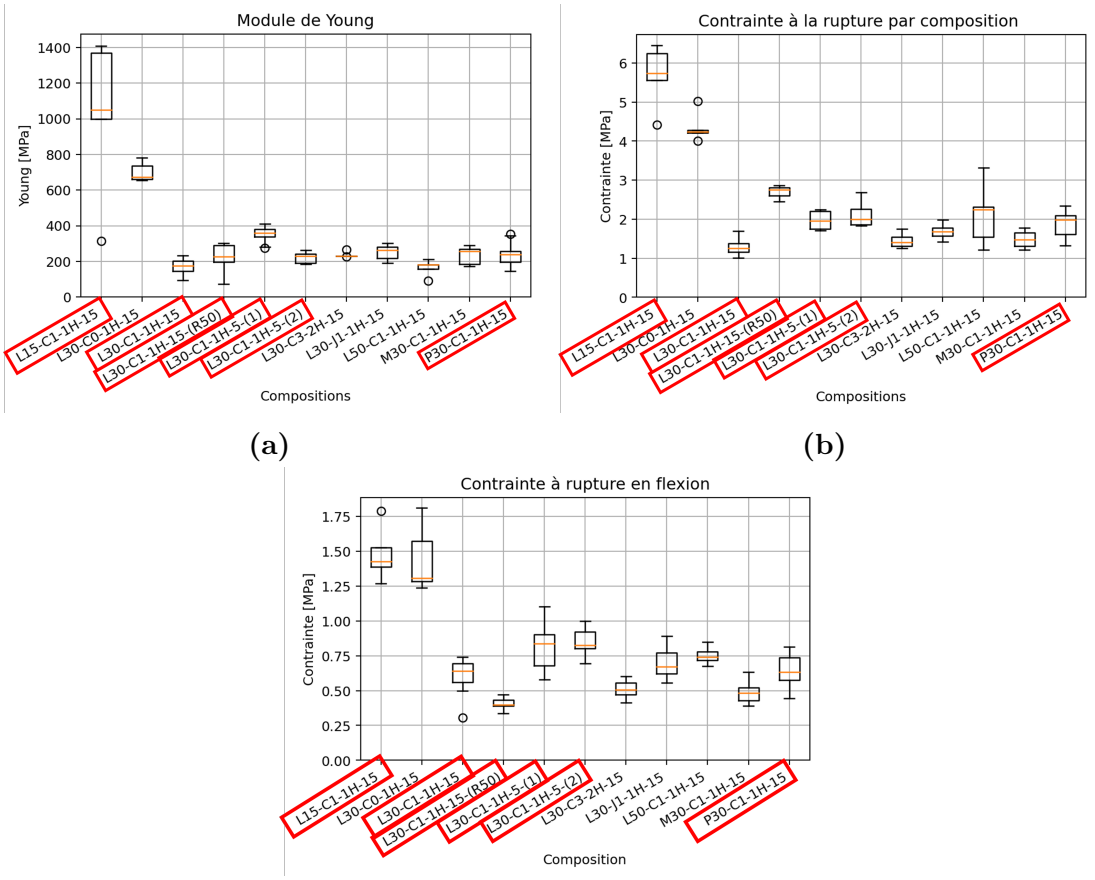

Figure 6.1: Figure 6.1a represents the average Young's modulus; Figure 6.1b represents the average compressive strength before fracture; Figure 6.1c represents the average tensile strength for each composition. (All graphs are made by Alexis and Eloise)

let's imagine a not well distributed material as in figure 6.2a. The reaction to a compressive load is not equal than for a better distributed material (figure 6.2b).

One can imagine that the material having a better distribution of paper along the whole compound will have a higher compressive strength than a material which is composed of big paper pellets.

However, composition with short mixing time (and so less distributed compositions than the reference composition) seems to provide better strength. The maximum stress obtained from the REF composition (long mixing time) is of

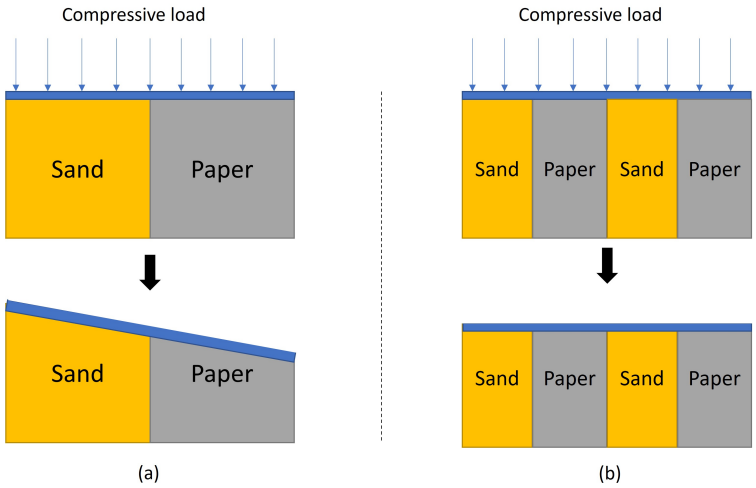

Figure 6.2: Example of reaction of a (a) not distributed and a (b) better distributed material to a compressive load

0.6 [MPa] while compositions L-5-1 and L-5-2 obtain flexural strengths values of 0.8 [MPa]. In this case, another parameter enters the equation: indeed, at the micro-scale, paper fibers in compositions L-5-1 and L-5-2 are longer, due to a smaller mixing time. Therefore, more entanglements are done in the material. Those entanglements have a positive effect on the material. Mechanical properties including strength and toughness are influenced by the number of entanglements. Indeed, longer paper filaments are providing ductility and strength to the material when the matrix cracks in flexion. For illustration, a material composed from long paper filaments as in figure 6.3a will retain the material from breaking (or failing catastrophically) better, than a material without long paper filaments.

Besides, composition R50 (made of 15% long fibers but also 15% of an undefined mix of paper since it comes from the recycled material) seems to have the worst bending behavior. An assumption made is that due to the second mixing of the recycled paper fibers, they are smaller than paper fibers mixed only once. Therefore, they form smaller paper filaments, giving lower flexural strengths to the material. However, composition R50 has better compressive strengths and Young's modulus than the reference composition. Indeed, the recycled mixture has already been compressed once, and therefore have a smaller porosity than REF (and therefore better compressive strength). For the same reason, composition L-5-2 has worse properties than composition L-5-1: the paper soaked during 48 hours

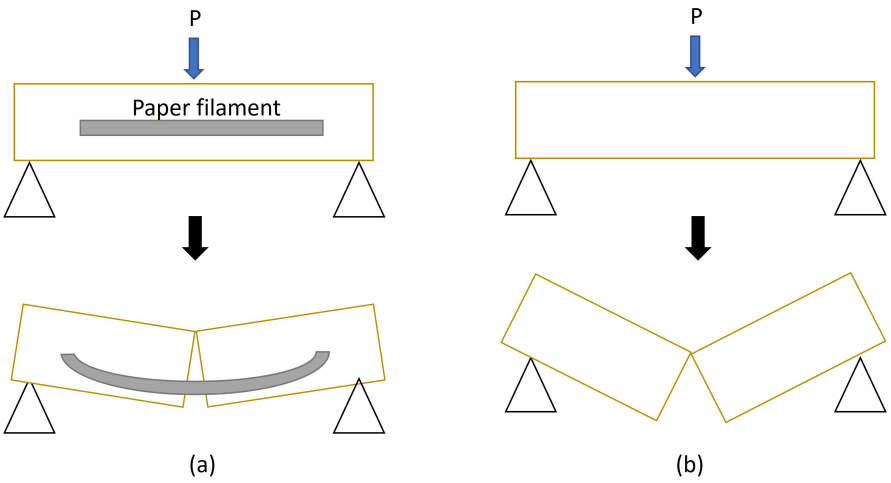

Figure 6.3: Example of reaction of a (a) with paper filaments composition (b) without paper filament composition.

(in composition L-5-2) is less resistant, and so the paper filaments are easier to break.

Finally, a last assumption is made: a linear microstructure is detrimental for the material properties. Indeed, composition P-E is composed of a completely linear structure, and obtain very low mechanical behaviors. Therefore, the short fiber or confetti compositions, P and P-E are the least interesting: they combine a fairly low stress at break with one of the lowest strain at break. One can assume that a fracture can easily propagate as it may be parallel to the linear structure around it.

6.1.2 Volume fraction

The reason to explain different mechanical behaviors for compositions L-5-1 and L-5-2 lies not only in the soaking time, but also in the volume fractions of the samples. Indeed, there is more sand and more lime in composition (1) while there is more air and more paper in composition (2). Therefore, the density of composition L-5-1 is greater than the density of composition L-5-2 in figure 6.4. This is another example proving that increasing sand and lime content, increase Young's modulus of the material.

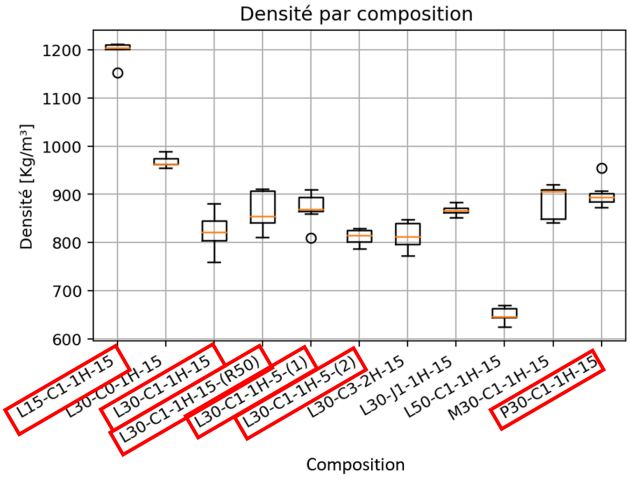

Figure 6.4: Comparative graph of the density of the different compositions. (Alexis and Eloise's graph)

In figure 6.4, it is observed that composition R50 is denser than the reference composition. Moreover, composition R50 is composed of a higher proportion of sand and lime and a lower proportion of paper and porosity than composition REF. The lower proportion of porosity can be explained by the recycled material that has already been compressed once. However, mechanical properties are worst for R50 composition than for REF composition. The main reason is explained in section 6.1.1 (smaller paper filaments). The conclusion is that the proportion of material is an influencing parameter, but the microstructure of the material is determining the mechanical properties of the material.

6.1.3 Porosity analysis

It has been shown that the molding process influences the ensuing microstructural morphology, and it is shown that constituent type, constituent proportion, porosity content and void topology affect a porous medium's bulk strength and elasticity in section 6.1.1. Therefore, the correlation between such observations caused additional investigation concerning the influence of porosity on the anisotropic mechanical properties of our components. 3D void topology (shape, size, and orientation) and interconnectivity were quantitatively investigated for the different compositions.

There is a difference between percolating and non-percolating materials: a percolating material allows water to flow through this material, which may be a good thing in some situations. Non-porous material instead, won't allow water to migrate through capillary action, so the water is absorbed and trapped, also causing diminished composite strength of the material. As none of the compositions tested are percolating, this could be a reason for the bad results of the water absorption test done in Mélanie's thesis [11].

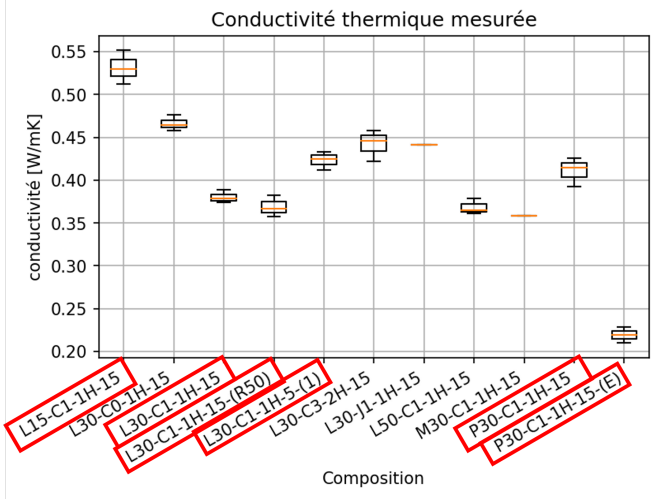

Figure 6.5: Results of the thermal conductivity tests done by Alexis and Eloise.

The most insulating composition is P-E, in which a large amount of undefined water was added to the mixture. The experimental findings indicate that this mixture, together with composition L15, have higher porosity in average. Porosity can be a quality for insulation, where the size and whether the pores are closed or open will determine the thermal transfer value of the material. Closed pores are better

insulators than open pores, and are mostly present in all compositions. Composition P-E is the richest composition in capillary pores (small closed pores), while composition L15 is the richest in coarse pores (larger closed pores) at interlayered locations. However, paper or recycled material aggregates would provide lower heat transfer. These two reasons can explain the large thermal conductivity differences, with a thermal conductivity of 0.22 W/mK for composition P-E and 53 W/mK for composition L15. All the other compositions have quite similar characters, with values between 36 and 46 W/mK.

So, interlayered closed pores offer a better insulation character to the material. Moreover, coarse closed pores and capillary closed pores are reducing the noise of a vacuum cleaner considerably, as shown in figure 6.6. With the most compressed composition (R50) showing better sound propagation, an other conclusion is that the sound propagation is dependent on the compressibility of the medium.

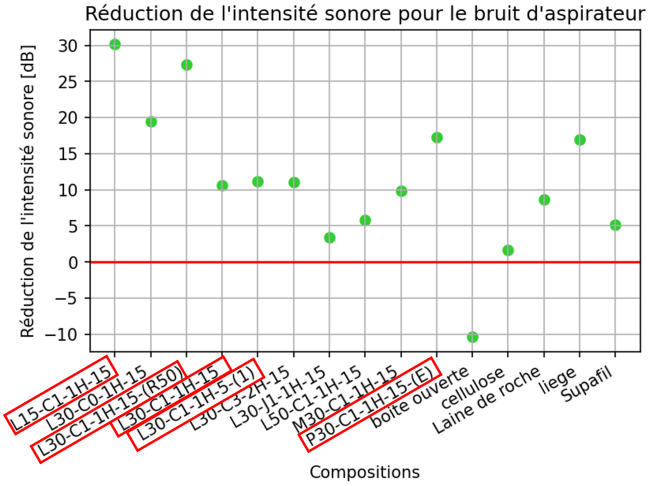

Figure 6.6: Noise reduction of a vacuum cleaner, made by Alexis and Eloise.

It is also shown that both reductions in elastic modulus and compressive capacity can be physically linked to the porosity metrics detected. Elasticity is dominated by porosity content and compressive capacity by the interrelation between porosity content, loading direction relative to the interlayer orientation, and the increased deformability of the composite configuration [30]. From the consideration and interpretation of these aspects, the anisotropic mechanical response of the samples was calculated. However, all samples have a similar anisotropic character. Indeed, none of them is made of spherical pores, and the orientation of the pores is quite similar in all compositions.

In general, in the different graphs obtained from Alexis and Eloise's thesis, as porosity increases:

- Density decreases
- Strength decreases slightly
- Thermal conductivity decreases
- Noise reduction increases

6.1.4 Compressibility of the material

To avoid unexpected failure, the ability to deform is useful. Indeed, as for polymers with a lot of entanglements, long paper fibers help restrain crack propagation as shown previously in section 6.1.1. Flexural ductility is an important parameter, and the flexural behavior approaches brittle behavior in most of the components tested. Once more, it is observed that the longer the paper filaments in the composition, the greater the deformation at break, and the better the flexural strength.

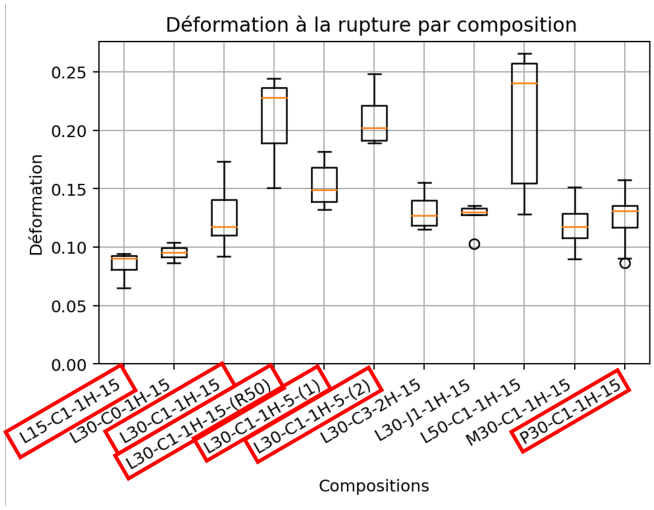

Figure 6.7

It is observed on figure 6.8 that the average Poisson's ratio value vary between 0.02 and 0.08 for the different compositions. None of the compositions stand out particularly, all of them give quite spread out and sometimes even negative Poisson's ratio

values. This means that the material appears to be globally compressible and that compression does not generate any consequent lateral expansion. This assumption is confirmed by the values of compressibility obtained. The instantaneous relative volume change of the components as a response to a pressure does not change tremendously.

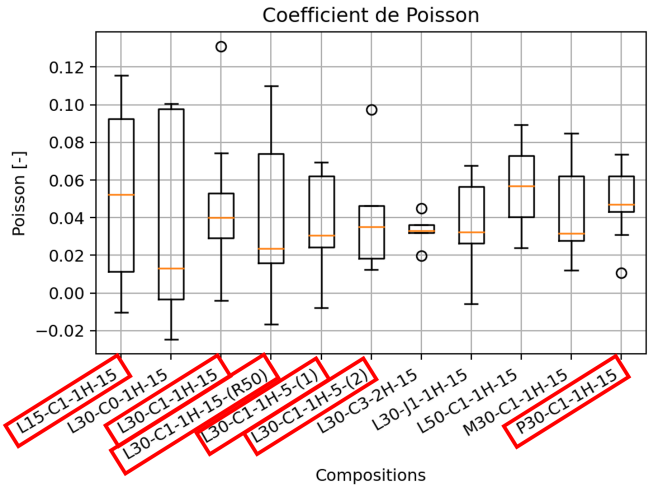

Figure 6.8: Poisson's coefficient comparative graph done by Alexis and Eloise.

Lower compressibility values are obtained for composition L15, and lower Poisson's ratio values are also obtained for this composition. This is explained because if the material has more sand grains, as the grains tend to shift rather than compact, it is very difficult to compact since it almost flows when compacting. Fine grained material like graded sand can be compacted to a high density, as much as 100% density, because the irregular fine grains don't flow or displace like larger gravels. The displacement of grains can be analysed using a Digital Volume Correlation function with the in-situ compression test, but this is an excessively long time and data demanding process.

6.2 Summary properties

Each parameter tested has some impact on the different tests. In this section the most important impacts of these parameters are presented:

1. **Paper length:** The main microstructural difference between long and short paper lengths, is the size of the paper filaments created in the composition. Long fibers (L) increase the length of the paper filaments, and therefore the ability of the material to deform in compression. Moreover, they provide ductility and strength to the material when the matrix cracks in flexion. Furthermore, the confetti's (P) tend to create, at microstructural scale, a more linear structure than long paper fibers. This is detrimental for the mechanical properties of the material.

2. **Material proportions:** The greater the quantity of paper, the lower the density, and the greater and bigger the paper filaments are observed in the compositions. Long fibers improve the ductility of the material, so the more they are, the better. The matrix formed by more sand and lime seems to bring a rather fragile behavior to the material. But the more the paper, the lower the mechanical strength of the material. Indeed, it is sand and lime that brings in the material mechanical resistance. The more sand and lime there is, the higher Young's modulus. It is therefore necessary to find a right balance between a sufficient quantity of sand and lime to ensure the mechanical strength of the material and a quantity that is not too great to limit the brittle behaviour. Finally, while porosity tends to stand on the paper fibers or interpolated by paper pellets, higher quantities of paper does not increase the porosity. Instead, more voids are found in the lower paper-composition. The voids have an effect on sound insulation performance, so a more porous material will insulate better.

3. **Mixing time:** The overall analysis of the results showed that the short mixing time (5min) brings better properties to the material than the longer mixing time (15min). This finding is the opposite result of the results presented in the first campaign. Indeed, a good ratio has to be found for the distribution of the paper in the material. A too low mix results in bad mechanical strengths due to the big paper pellets, while too long mixing time breaks the paper filaments which had a positive impact on the material behavior.

4. **Amount of water in the mix:** A large amount of water in the mix increases the porosity of the material. Indeed, More capillary pores (small pores) are present in the composition made with addition of water. The material shows a linear microstructure instead of a random microstructure and is therefore

more brittle. Its mechanical strength is then drastically decreased. However, this porous structure allows the material to better absorb sound and excel in terms of thermal performance. Indeed, porosity can be a quality for insulation, where the size and whether the pores are closed or open will determine the thermal transfer value of the material.

5. **Recycled composition:** This parameter is essential in the logic of circularity of this material. The findings allow some initial suggestions: Since the R50 composition contains 50% recycled material, the quantity of pores is reduced compared to the reference composition. Indeed, the recycled material is more compressed since it has already been compressed once. Therefore, a better Young's modulus and compressive strength are observed for this composition. However, paper fibers form smaller filaments due to second mixing. The flexural strength of the composition is then decreased.

6. **Paper soaking time:** Paper soaked in a water basin during 24 hours is optimal for the materials behaviour. The method "risotto" showed bad mechanical strengths, and paper soaked for longer times as well. Indeed, longer soaking times may reduce the resistance of paper, making it easier to break during the bending test.

6.3 Possible improvements

A list of possible improvements is provided here below:

- First of all, a method of uniform compression during molding should be implemented. Indeed, layer by layer molding results in coarse pores between layers. Furthermore, the different samples are not compressed with the same load, as it is done manually. This lead to differences in mechanical properties between samples, and can have a significant impact on the results.

- In some situations, a post-treatment of the material such as compression is considered to reduce the entrained air content in the sample by pressing the air out. The porosity is then lower in the composition. This is not favourable to all situations, as it leads to lower thermal insulation of the material as well.

- It could be interesting to perform a DVC analysis on every composition to have a better idea of the movement of every grain in the material at microscopic scale. The optimal size of sand grains can be found and a filtering method of crushed sand by size can be implemented. Furthermore, fractures happening in the samples can be identified and a solution can be implemented to limit some types of failures.

- Inserting graded (by size) crushed sand grains, to have some variability in sizes, can be of interest in the compression test. Indeed, graded sand can be compacted to a high density, as much as 100% density, because the irregular fine grains don't flow or displace like larger gravels.

- The phase correlation between paper and porosity can be analysed using a performing filtering method in Avizo. Knowing how the voids are created can help reducing them (or increasing there number in specific situations)

- An analysis of why lime is preferentially placed around sand, by analysing the chemical reaction between lime and crushed sand is a step to find better ratio's of lime/sand in the material.

- A method to manage the form of the paper fibers in the material is of interest. Indeed, longer paper filaments are giving better properties to the material than big paper pellets and small paper filaments. An idea is to introduce the paper in the mix in a specific manner, in the form of filaments.

Chapter 7

Conclusion

This study has taken a broad perspective at the possibilities of typical construction and demolition waste materials. Indeed, the composite studied in this thesis is a new building material that takes into account the various environmental, economic and social issues involved. The composite meets the main material characteristics needed for construction application, and can be adapted in specific situations. The proportion of material compounds in the composite is an influencing parameter, but the microstructure of the material is determining the mechanical properties of the material. Therefore, the combined use of computed tomography scans (CT-scans) and mechanical or thermal characterization tests of the composite material allowed relationships to be established between the microstructure and its macroscopic response.

Previously conducted studies that are applicable to materials for the construction industry as well as an introduction to computed tomography used in complex construction materials contribute to the fully understanding of this thesis. A visual representation of the microstructure is then provided together with its analysis, and the role and correlation of the different phases at microstructural scale are discussed. More information is given on the impact of the porosity in the samples and emphasis is given to the relationship between mechanical properties and pore size distribution and anisotropy. Through in-situ compression tests, the porosity at initial and final state and the compressibility is analysed, and a digital volume correlation approach is provided. Moreover, the results of the different laboratory tests made by Eloise and Alexis in parallel to this thesis are discussed by microstructural analysis. Finally, the discussion summarised the impact of the microstructural characteristics on the material and highlights the challenges to consider in further studies.

Appendix A

Segmentation

A.1 Median filter

The smoothing modules use lowpass filters to reduce the contrast and soften the edges of objects in an image. A lowpass filter lets low frequencies go through but attenuates high frequencies and noise. It reduces contrast but tends also to defocus the image. The gray levels of all pixels in the neighborhood are sorted from the smallest value to the largest one. The central pixel in the sort is then the median value, i.e. the value for which there are as many lower gray levels as higher ones. To explain this, consider the array:

$$\begin{bmatrix} 12 & 17 & 15 \\ 20 & 14 & 16 \\ 18 & 19 & 14 \end{bmatrix}$$

The sorted grey level values will be: 12 14 14 15 16 17 18 19 20 The median value is 16, and it will be the value of the output pixel. the module configuration is set to 3D.

Appendix B

Results

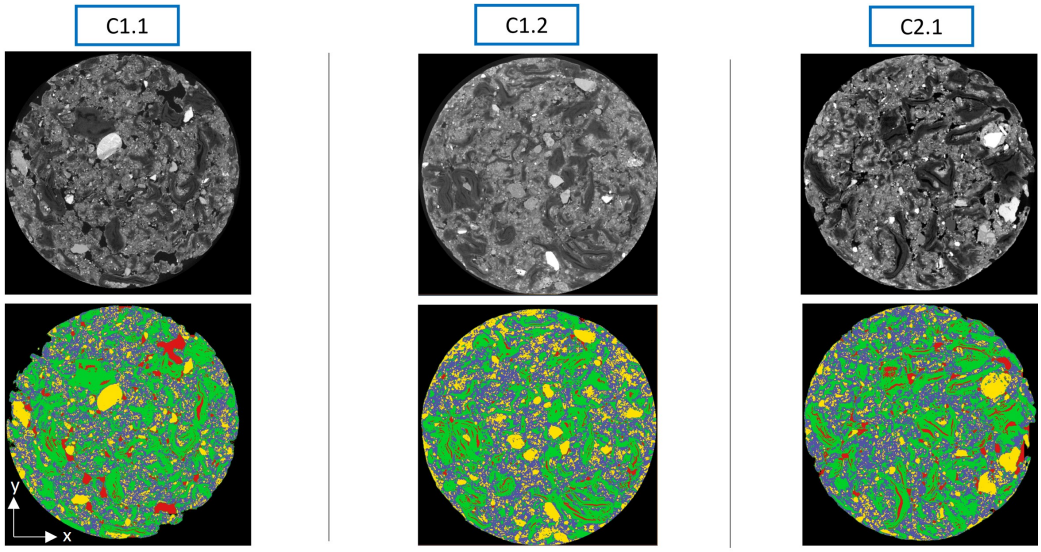

Figure B.1: XY-plan view of segmentation of the three samples of L-5-(1).

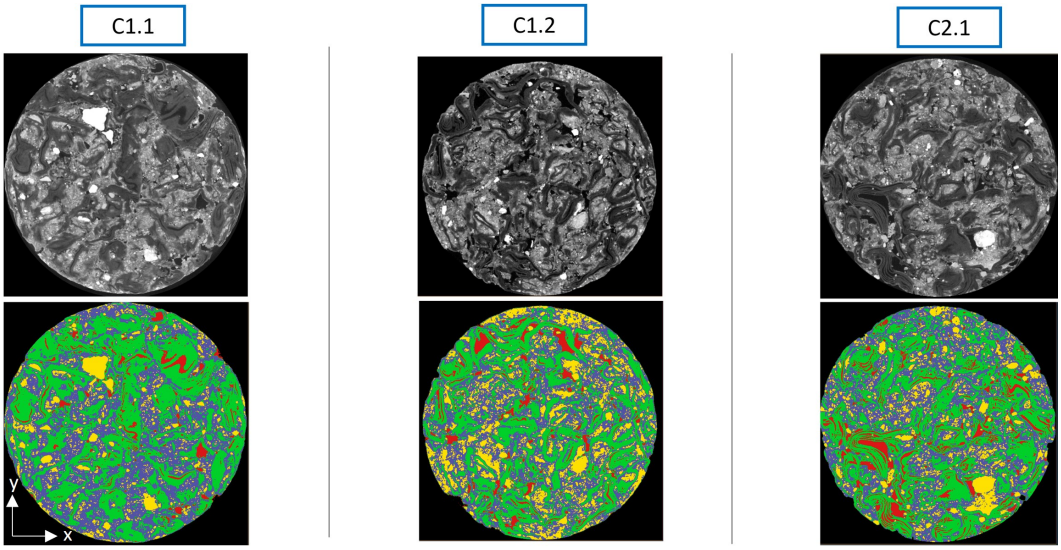

Figure B.2: XY-plan view of segmentation of the three samples of L-5-(2).

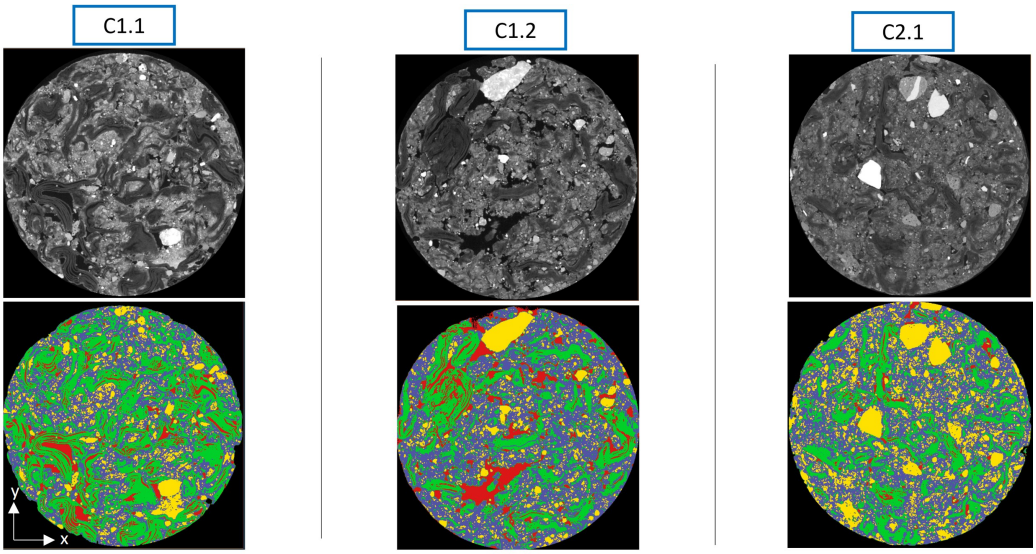

Figure B.3: XY-plan view of segmentation of the three samples of REF.

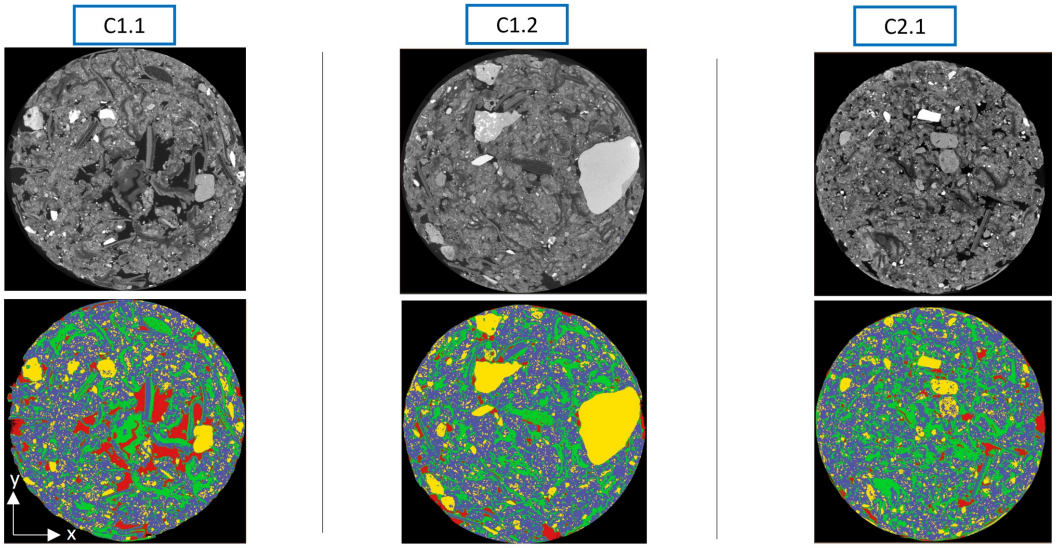

Figure B.4: XY-plan view of segmentation of the three samples of P.

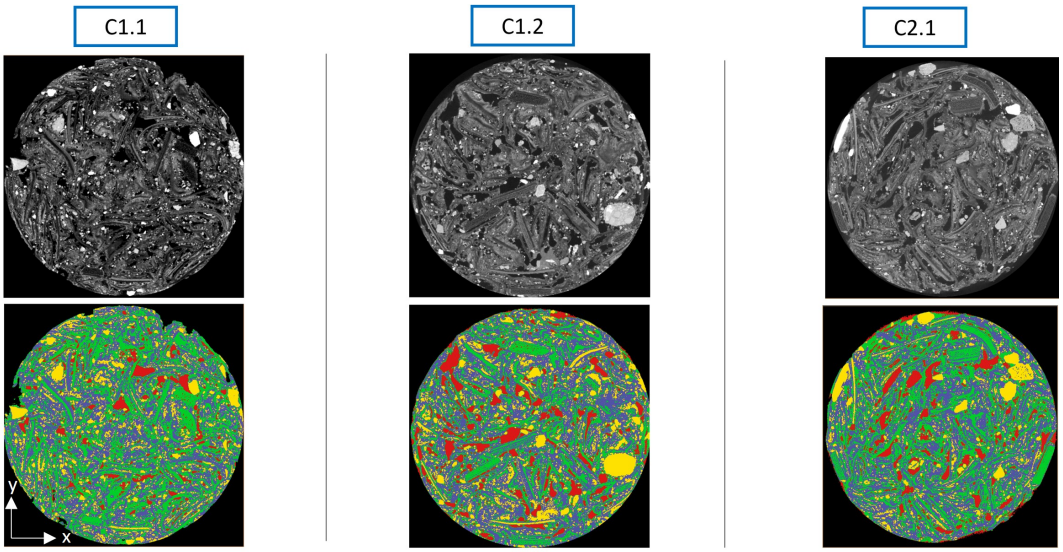

Figure B.5: XY-plan view of segmentation of the three samples of P-E.

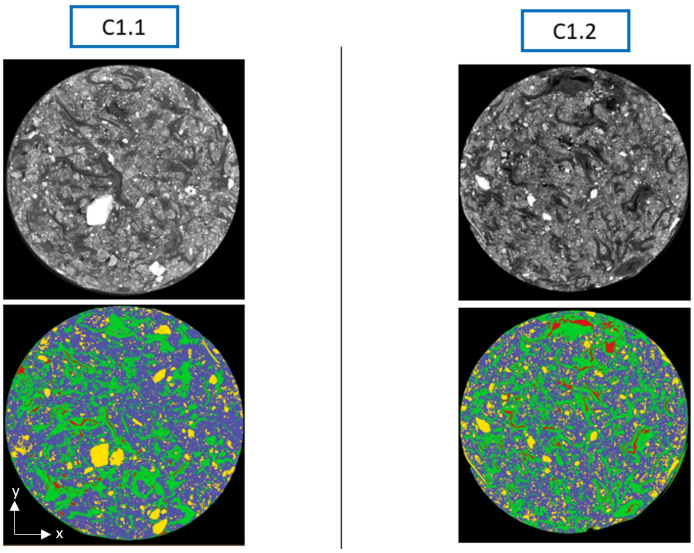

Figure B.6: XY-plan view of segmentation of the three samples of R50.

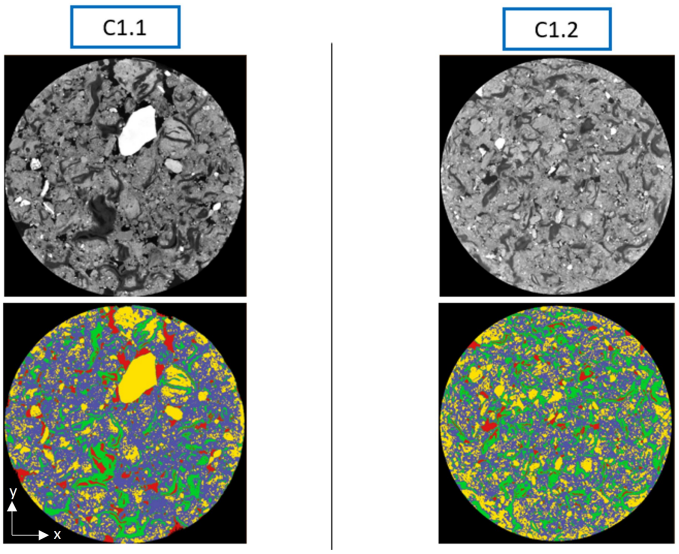

Figure B.7: XY-plan view of segmentation of the three samples of L15.

Appendix C

Volume fraction

C.1 Image analysis

	Porosity [%]	Paper [%]	Lime [%]	Sand [%]
L5-(1)-1.1	4	41	39	16
L5-(1)-1.2	4	36	42	18
L5-(1)-2.1	6	39	42	13
L5-(2)-1.1	5	43	42	10
L5-(2)-1.2	5	40	37	18
L5-(2)-2.1	9	43	37	11
REF-1.1	10	31	47	12
REF-1.2	9	38	41	12
REF-2.1	6	29	46	19
P-1.1	8	26	54	12
P-1.2	6	28	53	13
P-2.1	7	34	49	10
P-E-1.1	7	38	38	17
P-E-1.2	11	30	43	16
P-E-2.1	9	36	43	12
R50-1.1	6	24	47	23
R50-1.2	5	31	50	13
L15-1.1	6	15	61	18
L15-1.2	12	23	40	25

C.2 Experimental analysis

	Weight	addition of water	volume	volume without water	Specific gravity
Paper	1625	3550	5000	1450	1.1
Sand	6250	2775	5000	2225	2.8
Lime	5000	2450	5000	2550	2

Table C.1: Table for determining the specific gravity of the different compounds.

Appendix D

Porosity analysis

D.1 Void orientation

	Max. Feret diameter [°]	Min. Feret diameter [°]	Max. inertial moment [°]	Min. inertial moment [°]	Mean volume $[10^6 \mu m^3]$
L5-(1)-1.1	57	54	58	57	1,0
L5-(1)-1.2	58	55	58	56	1,1
L5-(1)-2.1	58	56	58	58	1,5
L5-(2)-1.1	58	53	59	55	2,5
L5-(2)-1.2	53	50	61	61	1,5
L5-(2)-2.1	58	55	58	56	2,0
REF-1.1	58	56	59	58	0,8
REF-1.2	55	50	58	60	1,2
REF-2.1	59	55	59	57	0,9
P-1.1	53	51	58	62	1,50
P-1.2	59	53	60	55	1,8
P-2.1	59	54	59	56	1,3
P-E-1.1	59	54	59	55	1,1
P-E-1.2	55	50	58	60	1,5
P-E-2.1	60	52	60	54	1,5
R50-1.1	59	53	59	55	1,1
R50-1.2	58	54	58	56	1,4
L15-1.1	60	51	61	53	2,2
L15-1.2	62	49	62	50	2,8

Table D.1: Table of capillary and coarse pores orientation for each sample.

	Max. Feret diameter [°]	Min. Feret diameter [°]	Max. inertial moment [°]	Min. inertial moment [°]
L5-(1)-1.1	68	38	69	39
L5-(1)-1.2	69	36	69	37
L5-(1)-2.1	72	40	70	39
L5-(2)-1.1	71	35	69	36
L5-(2)-1.2	74	41	74	40
L5-(2)-2.1	69	38	72	38
REF-1.1	68	38	69	38
REF-1.2	71	40	72	39
REF-2.1	70	39	71	37
P-1.1	74	37	73	38
P-1.2	72	38	74	38
P-2.1	68	36	68	38
P-E-1.1	73	37	72	39
P-E-1.2	69	40	70	40
P-E-2.1	68	38	69	38
R50-1.1	72	41	71	40
R50-1.2	71	37	70	36
L15-1.1	69	40	72	39
L15-1.2	72	39	74	40

Table D.2: Table of coarse pores orientation for each sample. (filter: volume of pores $10^6 \mu m^3$).

D.2 Pores size distribution

	Capillary pores ($< 10^5 \mu m^3$) [%]	Capillary pores ($10^5 - 10^6 \mu m^3$) [%]	Coarse pores ($> 10^6 \mu m^3$) [%]
L-5-1	58	34	8
L-5-2	54	34	12
REF	54	37	9
P	53	36	11
P-E	51	39	10
R50	52	37	11
L15	48	38	14

Table D.3: Pore Size Distribution. Volume fraction of capillary and coarse pores is represented for each composition.

Appendix E

Phase correlation

E.1 Methodology

It has been visually noticed in section 5.1 the evident formation of pores next to the paper fibers. Such porosity can significantly affect the behavior of the recycled compound. The question that this section try to answer is simple: Do the pores have a certain tendency to stay closer to the paper fibers? Or what is the correlation between paper and pores?
Two methods are then implemented to find results on this question:

E.1.1 Method 1: Neighbour count

The first method thought is a method based on counting the adjacent neighbours of paper and pores. The idea is so to find the ratio of "boundary" voxels from the pores that are in contact with paper. The next steps are followed:

1. First, coordinate of each paper and porosity voxel has to be collected. This is done by Aviso using the tool "arithmetics" to separated the objects previously segmented, and the data is saved under an excel-file.

2. The second step is to eliminate all voxels which are not boundary voxels of the pores. Indeed, This is done on Matlab by a simple Boolean. For each pore voxel, if at least one of the 6 neighbour (2 in the x-, y-, z-direction as seen on figure E.2) voxel is missing in the porosity excel then the voxel is considered as a boundary voxel and the Boolean returns "true". If none of the 6 voxels is missing, then the voxel is an "inside" voxel and is deleted for the further calculations.

3. The third step is counting the number of boundary voxels that are direct neighbours with paper-voxels, and the one that are neighbours with lime-

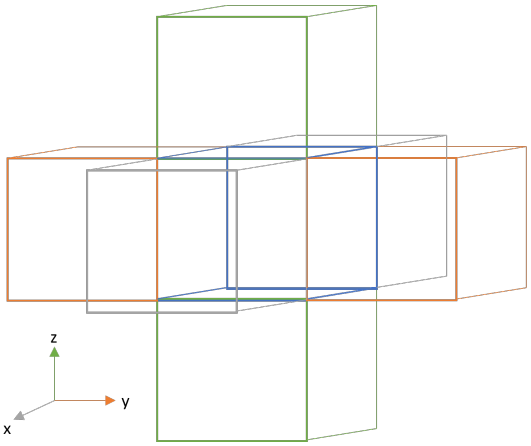

Figure E.1: The 6 neighbours of a voxel. The referential voxel is in blue; The two z-axis neighbours are in green; The 2 y-axis neighbours are in orange; The two x-axis voxel are in grey.

and sand-voxels.

4. a ratio is made for the neighbour voxels: (# of paper)/ (# of non-paper voxels).

E.1.2 Method 2: Modified PCF (bimodal with centroids) and method of quadrats

A classical way to analyze medium to large particles spacing is to use the radial distribution function (RDF), i.e. the probability for a neighboring particle to be located at a distance r, in any direction. However, the RDF analysis is not suitable if particles are preferentially aligned in a specific direction and the RDF analysis needs to be extended in order to take into account both distance and angular dependence of the particles spacing. This extended pair correlation function (PCF) is slightly modified here and has been directly applied to our 3D X-ray micro-tomography images.

PCF is defined, in 3D, as the probability for a given point [x,y,z] to be located inside a particle, given that another particle is located at the origin [0,0,0] [10]. In our case, this method will be applied with the centroids of each pore and paper fiber.

The RDF is constructed by drawing concentric circles at regular intervals around the centroid of a particle. The number of particle centroids falling in an annulus of radius r, N(r), is then divided by the area of the annulus. This procedure is then

repeated for each particle in order to determine N(r) as an average over all the particles, N(r).

Now, the radius r has to be defined. Indeed, we have to define a measure-

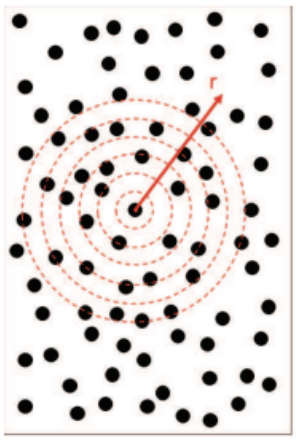

Figure E.2: Principle of RDF analysis for a random distribution [10].

ment frame. This size of frame corresponds to the maximum distance r at which the RDF is computed. To know this distance, the Method of quadrats is used.

Method of quadrats:
A quadrat is a small, designated portion of the entire area to be sampled that is marked off so that the population within it can be counted. Estimated average density $= \frac{\#individuals}{\#quadrats \cdot A}$ with A the area of a quadrat [9]. This method is used to find a representative radius r. However, this technique is in 2D and has to be applied in 3D. Furthermore, a radius has to be found so a quadrat (square) is transformed in a sphere. So, the method is the following:

1. First of all, the biggest possible sphere is taken from the sample and the volume fraction is noted.

2. Then the radius of the sphere is divided by 2 in all directions. The volume fraction is taken again. If this volume fraction is not representative of the volume fraction of the initial cube, than the radius of this sphere will be used for the RDF.

3. If the volume fraction of the sphere is still representative of the total volume fraction in the sample, then the sphere is again divided by 2, 4, 8 and the same happen again until the radius is found.

Counting procedure of the RDF: The center of the measurement frame is moved to the centroid of a first pore. Each voxel of the measurement frame occupied by paper particles is equal to one and all the other voxels occupied by the matrix, sand and porosity are equal to zero. The measurement frame is then moved to the location of a second pore, a similar counting is performed and the counts are then added up and so on for all particles. This value, between 0 and 1, corresponds to the local volume fraction associated to a pore and its near environment. This local volume fraction is additionally normalised by the global paper and porosity volume fraction over the entire image. This normalised value is called the PCF. For a perfectly homogeneous spatial distribution, the PCF would be equal to 1 for each point. A PCF value smaller or larger than 1 corresponds thus respectively to a smaller or larger probability to find paper as a neighbour in the vicinity of a pore compared to a perfectly homogeneous distribution. So, if there is a correlation between pores and paper, the value of the PCF should be more than 1.

E.2 Results

E.2.1 Method 1: Neighbour count

The results got with this method are all close to 100%, while it is clearly observed in the segmented images that the pores are not only in contact with paper. The method didn't worked due to the filtering step. Indeed, the boundary between voids (dark voxels) and sand or lime (white voxels) is transformed during median filtering to a grey voxel, which represent paper. Therefore, all pores boundaries where marked with paper voxels. Filtering is however necessary to reduce noise. If noise is not reduced, black voxels are appearing inside every material component and the results are then not representative of the reality. Better results should be obtained with a better method of filtering, but those type of filtering demand excessive time and data. The correlation between sand and lime could also be interesting to analyse.

E.2.2 Method 2: Modified PCF (bimodal with cen- troids) and method of quadrats

The results obtained with this method are meaningless for two reasons:

1. First of all, this method should have worked if the pores and paper fibers were more or less spherical. However, this is the case for none of the compositions made during this project. Indeed, the paper fibers as well as the pores are elongate, and completely anisotropic. Therefore, the extremity of a long paper fiber is sometimes far from its bary-center, and thus the data acting close to this extremity will not be calculated.

2. Secondly, there are huge differences between the size of the pores and paper fibers. This is a problem since pores that have the size of a voxel are counted as 1, and pores larger than $1mm^3$ are also counted as 1.

This method being to difficult to implement perfectly, it is abandoned.

Appendix F

Compressibility

F.1 Poisson's ratio

The Poisson's ratio (= lateral strain/axial strain) allows us to see if the material is compressible or not (v∈ [0,0.5] if v=0.5 then the material is incompressible).

$$Poisson's\,ratio\,(v) = \frac{lateral\ strain}{axial\ strain} = \frac{1 - \frac{d}{d_0}}{\frac{l}{l_0} - 1}$$

However, this one could not be found for the different compositions, as it has to be calculated during the elastic phase, and the dimensions of the data received from the in-situ tests are deformed. Therefore, the Poisson's ratio values could not be calculated, as it is depending of the difference in height between before and after compression of the sample.

Bibliography

[1] Claudiu Aciu, Dana Adriana Iluţiu-Varvara, Nicoleta Cobirzan, and Anca Balog. Recycling of paper waste in the composition of plastering mortars. *Procedia Technology*, 12:295–300, 2014.

[2] K Anandaraju, B JoseRavindra Raj, and R VijayaSarathy. Experimental investigation of papercrete brick. *International Journal of Machine and Construction Engineering*, 2(2):2394–3025, 2015.

[3] SN Aqida, Mohd Imran Ghazali, and J Hashim. Effect of porosity on mechanical properties of metal matrix composite: an overview. *Jurnal Teknologi*, pages 17â–32, 2004.

[4] J-Y Buffiere, E Maire, J Adrien, J-P Masse, and E Boller. In situ experiments with x ray tomography: an attractive tool for experimental mechanics. *Experimental mechanics*, 50(3):289–305, 2010.

[5] Kunyang Chen, Jiayuan Wang, Bo Yu, Huanyu Wu, and Jingrong Zhang. Critical evaluation of construction and demolition waste and associated environmental impacts: A scientometric analysis. *Journal of Cleaner Production*, 287:125071, 2021.

[6] Gerald Chik. Specific gravity vs. bulk density. 04 2015.

[7] TW Clyne and James Edward Campbell. *Testing of the Plastic Deformation of Metals*. Cambridge University Press, 2021.

[8] Huabo Duan and Jinhui Li. Construction and demolition waste management: China's lessons, 2016.

[9] Henry Allan Gleason. Some applications of the quadrat method. *Bulletin of the Torrey Botanical Club*, 47(1):21–33, 1920.

[10] Florent Hannard. *3D characterization, modelling and tailoring of microstructure heterogeneity effects on damage and fracture of 6xxx aluminium alloys*. PhD thesis, UCL-Université Catholique de Louvain, 2018.

[11] Mélanie Horvath, Thomas Pardoen, João Saraiva Esteves Pacheco De Almeida, Geoffrey Van Moeseke, and Benoit Thielemans. La brique de papier et son application en architecture.

[12] Mélanie Horvath, Sophie Trachte, and Thomas Pardoen. New circular building composite material to upcycle building wastes. In *Journal of Physics: Conference Series*, volume 2042, page 012167. IOP Publishing, 2021.

[13] NJ Jarvis. A review of non-equilibrium water flow and solute transport in soil macropores: Principles, controlling factors and consequences for water quality. *European Journal of Soil Science*, 58(3):523–546, 2007.

[14] William F Laurance. The value of trees. *New Scientist*, 2006.

[15] MB Leite and PJM Monteiro. Microstructural analysis of recycled concrete using x-ray microtomography. *Cement and Concrete Research*, 81:38–48, 2016.

[16] Zhiheng Liu, Xudong Chen, Peng Wu, and Xiyuan Cheng. Investigation on micro-structure of self-compacting concrete modified by recycled grinded tire rubber based on x-ray computed tomography technology. *Journal of Cleaner Production*, 290:125838, 2021.

[17] Y-W Mai and B Cotterell. Porosity and mechanical properties of cement mortar. *Cement and Concrete Research*, 15(6):995–1002, 1985.

[18] Maria Menegaki and Dimitris Damigos. A review on current situation and challenges of construction and demolition waste management. *Current Opinion in Green and Sustainable Chemistry*, 13:8–15, 2018.

[19] Leonardo FR Miranda, Camila S Constantino, Carla R Monich, and Antônio A de M. Neto. Use of recycled sand produced at construction sites in bedding mortars. *Journal of materials in civil engineering*, 25(2):236–242, 2013.

[20] Mardiha Mokhtar, Nor Baizura Hamid, Masiri Kaamin, Muhammad Nur Aiman Adnan, Muhammad Amzar Othman, Muhammad Shahruzi Mahadzir, and Mah Mudin Amin. Investigating the utilisation of plastic bottle as aggregate replacement for concrete block. In *Journal of Physics: Conference Series*, volume 1049, page 012093. IOP Publishing, 2018.

[21] Jordi Pinart Noguera. Estudi dels efectes de la introducció d'additius i modificacions estructurals en el procés d'assecatge dels panells honext. B.S. thesis, Universitat Politècnica de Catalunya, 2021.

[22] Tefy Raoelivololona, Mamiharijaona Ramaroson, and Chrysostome Raminosoa. Paper recycling for the making of constructions materials. In *MATEC Web of Conferences*, volume 307, page 01041. EDP Sciences, 2020.

[23] Rafael A Robayo-Salazar, William Valencia-Saavedra, and Ruby Mejía de Gutiérrez. Construction and demolition waste (cdw) recycling—as both binder and aggregates—in alkali-activated materials: A novel re-use concept. *Sustainability*, 12(14):5775, 2020.

[24] Sina Safinia and Amani Alkalbani. Use of recycled plastic water bottles in concrete blocks. *Procedia engineering*, 164:214–221, 2016.

[25] Yogesh D Shermale and Mahaveer B Varma. Properties of papercrete concrete: Building material. *IOSR Journal of Mechanical and Civil engineering*, 14(02):27–32, 2017.

[26] Diego Soto-Gómez, Laura Vázquez Juíz, Paula Pérez-Rodríguez, J Eugenio López-Periago, Marcos Paradelo, and John Koestel. Percolation theory applied to soil tomography. *Geoderma*, 357:113959, 2020.

[27] Shitaw Tafesse, Yidnekachew Esayas Girma, and Eliyas Dessalegn. Analysis of the socio-economic and environmental impacts of construction waste and management practices. *Heliyon*, page e09169, 2022.

[28] Ganesh Tapkire, Pramod Patil, and Hemraj R Kumavat. Recycled plastic used in concrete paver block. 2014.

[29] ML Thomson, JE Lindqvist, Jan Elsen, and CJWP Groot. Porosity of historic mortars. In *13th international brick and block masonry conference Amsterdam*, 2004.

[30] Marchant van den Heever, Anton du Plessis, Jacques Kruger, and Gideon van Zijl. Evaluating the effects of porosity on the mechanical properties of extrusion-based 3d printed concrete. *Cement and Concrete Research*, 153:106695, 2022.

[31] Lívia Vásárhelyi, Z. Kónya, Ákos Kukovecz, and Robert Vajtai. Microcomputed tomography–based characterization of advanced materials: a review. 2020.

[32] Miguel A Vicente, Jesús Mínguez, and Dorys C González. The use of computed tomography to explore the microstructure of materials in civil engineering: from rocks to concrete. *Computed tomography-advanced applications*, pages 207–230, 2017.

[33] Wikipedia contributors. Percolation — Wikipedia, the free encyclopedia, 2022. [Online; accessed 31-May-2022].

[34] Harith Zaki, Iqbal Gorgis, and Shakir Salih. Mechanical properties of paper-crete. In *MATEC Web of Conferences*, volume 162, page 02016. EDP Sciences, 2018.

UNIVERSITÉ CATHOLIQUE DE LOUVAIN
École polytechnique de Louvain
Rue Archimède, 1 bte L6.11.01, 1348 Louvain-la-Neuve, Belgique | **www.uclouvain.be/epl**